Best practice guide for the assessment of EMF exposure from vehicle Wireless Power Transfer systems

EMPIR
The EMPIR initiative is co-funded by the European Union's Horizon 2020 research and innovation programme and the EMPIR Participating States

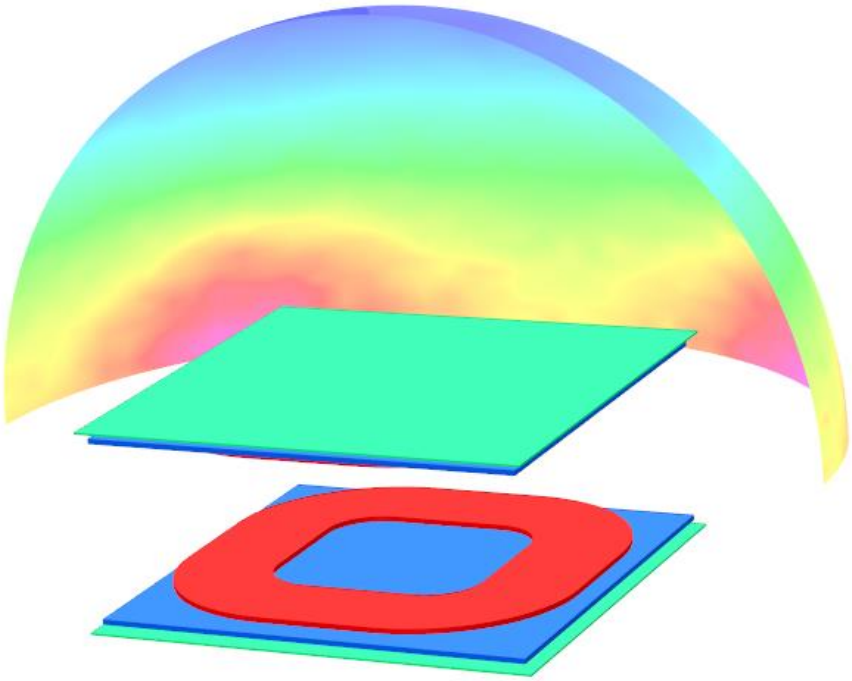

Best practice guide for the assessment of EMF exposure from vehicle Wireless Power Transfer systems

JRP 16ENG08 Metrology for Inductive Charging Of Electric Vehicles (MICEV)
https://www.micev.eu/

ISBN 978-88-945324-1-8

Best practice guide for the assessment of EMF exposure from vehicle Wireless Power Transfer systems

Edited by:

Roberta Guilizzoni (NPL)
Stuart Harmon (NPL)
Mauro Zucca (INRIM)

Authors:
Peter Ankarson (RISE)
Oriano Bottauscio (INRIM)
Bob Clarke (NPL)
Fabio Freschi (POLITO)
Roberta Guilizzoni (NPL)
Stuart Harmon (NPL)
Erika Laporta (CIRCE)
Lionel Pichon (CNRS
Jorge Bruna Romero (CIRCE)
Luca Zilberti (INRIM)
Mauro Zucca (INRIM)

Affiliations:
CIRCE, Centro de investigacion de recursos y consumos energeticos, Zaragoza, Spain.
CNRS, Centre National de la Recherche Scientifique, Paris, France.
INRIM, Istituto Nazionale di Ricerca Metrologica, Turin, Italy.
NPL, National Physical Laboratory, Teddington, United Kingdom.
POLITO, Politecnico di Torino, Turin, Italy.
RISE, Research Institutes of Sweden, Borås, Sweden.

How to cite this document
16ENG08 EMPIR MICEV consortium, "*Best practice guide for the assessment of EMF exposure from vehicle Wireless Power Transfer systems*", 2021, Edited by R. Guilizzoni, S. Harmon, M. Zucca.
ISBN: 978-88-945324-1-8, available online at: https://www.micev.eu/

Notice to reader
This technical document is a snap-shot of the current situation. It was produced as part of a research project and will not be updated. By its nature its validity is time-limited, and will require the reader to evaluate this guide's content based on the future changes in technology and that of the related standards.

February 17, 2021
ISBN: 978-88-945324-1-8

The EMPIR initiative is co-funded by the European Union's Horizon 2020 research and innovation programme and the EMPIR Participating States

Contents

1. Introduction

This document is based on the experience gained by the partners involved in the EMPIR Project 16ENG08 "Metrology for inductive charging of electric vehicles (MICEV)" (www.micev.eu). The project addressed the electromagnetic metrology and human exposure problems related to inductive charging of electric vehicles, both from a modelling and a measurement point of view.

The guidelines reported here are designed for people who approach the assessment of human exposure in vehicles and around inductive charging stations.

These guidelines are intended to complement the published standards in use and those currently being developed by international technical organisations and bodies.

This document concerns the charging of electric vehicles, for transmitted power up to 200 kW. The frequency range of interest is related to resonant coils that produce significant electromagnetic field (EMF) emissions from the charging station. Resonant coils operate in the frequency range between 20 kHz and 85 kHz. Their electric current, and thus the magnetic field and harmonic distortion, is very low and not significant in relation to human exposure guidelines. Consequently, the frequency range of interest for human exposure does not exceed 100 kHz. This guide seeks to assemble the experience gained in the field of human exposure assessment and to provide information for the assessment of exposure through experimental measurements and validated calculations. The calculation of the induced quantities, in particular the induced electric field and electric currents in the tissues, is of fundamental importance for the determination of human exposure. From the point of view of dosimetry, for obvious reasons of feasibility, the calculation replaces the measurement. Therefore, a whole chapter of this guide covers the choice of instruments and the description of the correct settings for both the magnetic field calculations and the dosimetric calculations.

The document particularly focuses on the following challenges:

- the testing framework, including the common layout of charging stations, with reference to the normative and EU Directive on magnetic field exposure (Sections 4 to 6);
- means and methods to perform:
    - measurements of the magnetic flux density in and around a vehicle;
    - measurements of limb currents (Section 7);
- means and methods to perform:
    - analytical calculation of magnetic flux density levels for EMF exposure assessment;
    - computation of the induced electric fields in human beings (Section 8).

The guidelines contain some appendices, which include the following: a real example of a charging station; some tables with the exposure limits referred to in this guide; a brief comparison between two existing standards; a test case of a numerical code to calculate the sources; some results on the sensitivity of simulated exposure metrics to the variations in tissue properties and, finally, the measurement capabilities of European national metrological institutes concerning AC magnetic fields at the frequency range of interest for Wireless Power Transfer systems (WPTs).

These guidelines do not intend to discuss the implementation of wireless charging systems, the design of their components or the optimisation of their performance, as they do not discuss the interoperability or the techniques for building the systems, or their classification.
Risk analysis and mitigation measures are beyond the scope of this guide.

2. Scope

The scope of this guide is:

- to outline the required steps to determine compliance of an inductive charging system;
- to conduct human exposure assessment;
- to calculate and measure the magnetic field around the system.

Particular emphasis was given to measurement and computational accuracy, with the purpose of providing information on dosimetric calculations.

This document is intended to be used for vehicles that are statically charged, as dynamic charging, occurring when the vehicle is in motion, requires the addition of specific operations and/or devices, for both the in-field measurement and analytical calculations.

The frequency range is up to 100 kHz, with transmitted powers up to 200 kW.

The document refers to the ‘general public’ exposure limits, which are more stringent than ‘occupational’ exposure limits.

3. Definitions

Dynamic charging: a type of inductive power transfer charging in which the vehicle moves whilst being charged.

Electric field strength (*E*): vector quantity whose numerical value coincides with the numerical value of the force experienced by a unit, positive, point charge that, in the adopted reference frame, is at rest. It is expressed in volts per metre (V/m). A distinction must be made between the environmental electric field and the electric field present in body tissue as a result of exposure to the environmental electric field.

Electric vehicle (*EV*): a vehicle operating by means of an electric motor, instead of an internal-combustion engine that generates power by burning a mix of fuel and gases. Depending on the degree by which electricity is used as an EV's energy source, there are three types of EVs: battery electric vehicles (BEV), plug-in hybrid electric vehicles (PHEV), and hybrid electric vehicles (HEV).

Inductive power transfer (*IPT*) system, also called "**wireless power transfer (*WPT*)** system": a system formed by two electrically isolated coils magnetically coupled through air, capable of transmitting power at a certain efficiency rating.

Limb current: the electric current induced in the limbs of a human exposed to electromagnetic fields resulting either from contact with an object in an electromagnetic field or else the flow of capacitively induced currents in the exposed body. It is expressed in amperes (A).

Magnetic field strength (*H*): vector quantity obtained at a given point by subtracting the magnetization M from the magnetic flux density B divided by the magnetic constant μ_0. It is expressed in ampere per metre (A/m).

Magnetic flux density (*B*): vector quantity, expressed in tesla (T), which allows quantifying the force ***F*** experienced by a point charge q, moving at velocity ***v*** in the adopted reference frame, as $\boldsymbol{F} = q(\boldsymbol{E} + \boldsymbol{v} \times \boldsymbol{B})$, where ***E*** is the local electric field measured in that reference frame according to the definition given above. It is expressed in tesla (T). In free space and in biological materials, magnetic flux density and magnetic field strength can be related by using the equation $B = \mu_0 H$, where μ_0 is the vacuum permeability. For a magnetic field strength of H = 1 A/m, B is approximately equal to 1.25 μT.

Primary or transmitting coil (*Tx* coil): a coil in which an AC current flows, thus generating an AC magnetic field (primary field).

Secondary or receiving coil (*Rx* coil): a coil in which a voltage is generated, by the AC current flowing in the primary coil, according to Faraday's law of induction.

Static charging: a type of WPT charging in which the vehicle does not move whilst being charged.

4. WPT charging stations

A typical power transfer system functioning through inductive coupling is a system formed by two electrically isolated coils magnetically coupled through the air, being capable of transmitting power with a specified efficiency. Contactless Inductive or Wireless Power Transfer (WPT) systems have many advantages when compared to traditional charging systems, in terms of electric shock risk and ease of vehicle charging. One disadvantage of these systems is the potential safety risk associated with electromagnetic field and limb current exposure, which needs to be assessed.

The WPT systems for electric vehicles (EVs) have a fixed secondary system that allows for a range of distances "h" between the primary and secondary windings as shown in Figure 1. Common distances between coils range from 100 mm to 300 mm. In some WPT systems, the dimensions of the primary and secondary coils are comparable to increase the compactness of the design.

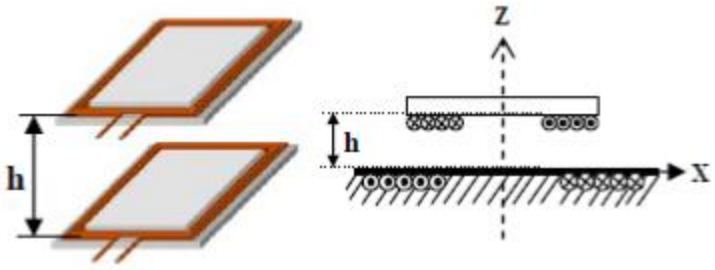

Figure 1. Schematic of transmitting (Tx) and receiving (Rx) coils.

The working modes of WPT systems applied to EV charging can be classified as either (1) static or stationary WPT: the vehicle does not move during charging; or (2) dynamic WPT: the vehicle moves along a suitable roadway whilst being charged. This document refers to static charging.

The general schematic of a WPT charging station is shown in Figure 2.

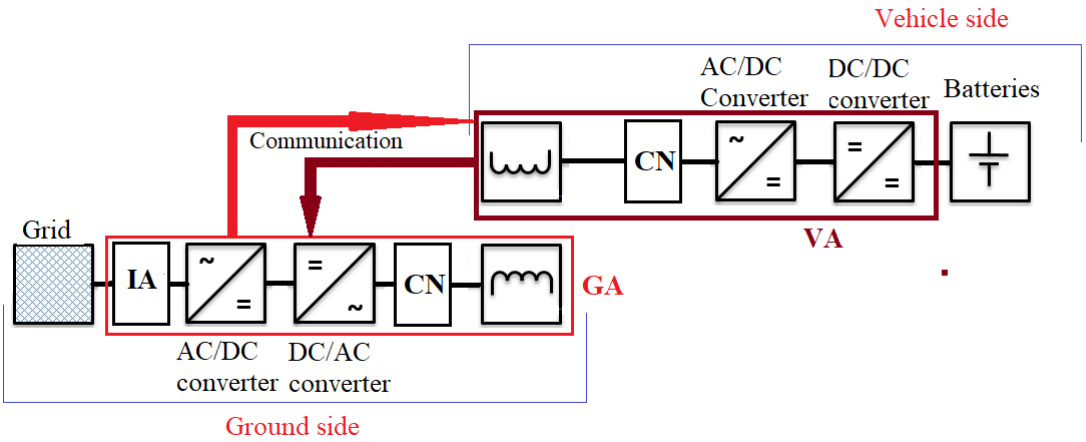

Figure 2. Typical WPT charging system. Scheme of the ground assembly (GA) and of the vehicle assembly (VA).

On the ground (transmission) side, there is an electric input access (IA), which can include an insulation transformer, and EMI filters and power factor correction electronics. Usually, two power converters are present and sometimes a compensation network (CN) driving the transmitter coil (Tx). All these components, including the communication electronics between the ground and the vehicle are called the ground assembly (GA). Similarly, for the receiver coil (Rx), a CN and on-board power converters, including the communication electronics between the vehicle and the ground are called the vehicle assembly (VA).

The main sources of magnetic field emissions are the primary and secondary coil currents. Their relative dimensions can differ, as is the case for heavy vehicles, such as trucks and buses (Figure 3).

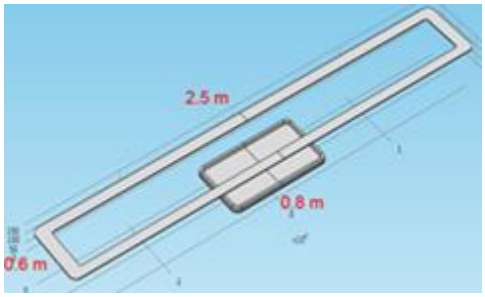

a)
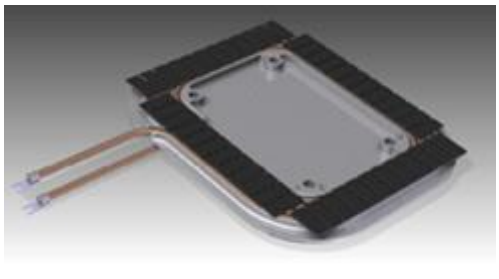
b)

Figure 3. a) Bus Tx and Rx WPT coils (isometric view) and b) Tx 3D CAD design.

To increase transmission efficiency and reduce stray fields, the coils are equipped with:

- flux concentrators made from soft magnetic materials, typically ferrite;
- magnetic screening, typically a high conductive aluminium material.

A WPT system needs to be able to support robust communication between the GA and the VA. It needs to provide the output power safely without overheating, even in the presence of foreign objects (FO) between the coils, and it needs to be compliant with EMC and EMI requirements. Especially in the case of light vehicles, the system should be interoperable. Standard SAE J2954 [1] provides classification and requirements for Light-Duty Plug-in/Electric Vehicles. A more detailed example of a charging station layout is described in Appendix A.

Another important requirement is the compliance with electromagnetic field (EMF) exposure of human beings especially when implanted medical devices (IMDs) are present. This topic is addressed in Section 8.2.7.

5. Normative references for WPT systems

There are many standards that can cover the WPT of electric vehicles, the main standards are listed below.

- **SAE J2954** [1]. This is a standard for vehicle WPT systems. It aims to establish minimum performance and safety criteria for wireless charging of electric and plug-in vehicles. SAE J2954 also focuses on standardising the interface to improve interoperability and develop procedures for subsystems to communicate. Its topics cover: Testing, Minimum efficiency, Positioning of the vehicle and charging unit, Potential locations for residential and on road charging, Frequency, Communications and software, Interoperability and Safety.
- **IEC 61980** [2-4] "Electric vehicle wireless power transfer systems", consisting of 3 parts: 61980-1 General requirements for all inductive charging systems; 61980-2 Requirements for communication between EV and infrastructure with respect to WPT systems and 61980-3 Requirements for the magnetic field power transfer systems.
- **IEC 61000** "Electromagnetic compatibility (EMC)" consisting of 6 parts, IEC 61000 contains general EMC requirements. The most relevant chapters are IEC 61000-3-4 [5] and IEC 61000-3-5 [6] which specify the limits on emission of harmonic currents and voltage for current levels greater than 16 A per phase. IEC 61000 parts 6-3 [7] is the generic standard for emission for residential, commercial and light-industrial environments.
- **IEC PAS 63184 ED1: "**Assessment methods of the human exposure to electric and magnetic fields from wireless power transfer systems - Models, instrumentation, measurement and numerical methods and procedures (Frequency range of 1 kHz to 30 MHz)". To date, it is still a draft document at the working groups, but it promises to be a reference document in this field.
- **CISPR 11** [8] "Industrial, scientific, and medical equipment – Radio-Frequency disturbance characteristics – Limits and methods of measurement" is an International Standard for electromagnetic emissions (disturbances) from industrial, scientific and medical (ISM) equipment, from 150 kHz to 30 MHz.
- **CISPR 12** [9] "Radio disturbance characteristics - Limits and methods of measurement for the protection of off board receivers". This standard applies to vehicles, boats and internal combustion engines. The limits are designed to provide protection for transmission receivers in the frequency range of 30 MHz to 1000 MHz (IEC 2010).
- **CISPR 25** [10] The standard aims to regulate radio disturbance characteristics for the protection of on-board receivers. It includes limits and procedures for the measurement of radio disturbances in the frequency range of 150 kHz to 1000 MHz. It applies to vehicles, boats and internal combustion engines.
- **ISO 16750** [11] "Road vehicles — Environmental conditions and testing for electrical and electronic equipment", Part 2: Electrical loads.
- **ISO 26262** [12]. This is a functional safety standard for road vehicles which addresses potential failures in electrical and electronic systems and develops a structure for hazard elimination (ISO, 2014).
- **ISO 6469**. This standard contains safety specifications for electrically propelled road vehicles. It includes electrical, mechanical and safety rules for electric vehicles. It consists of 3 parts: ISO 6469-1:2009; electrically propelled road vehicles, safety specifications part 1 [13]: on-board rechargeable energy storage system; ISO 6469-2:2009; electrically propelled road vehicles, safety specifications Part 2 [14]: vehicle operational safety means and protection against failures and ISO 6469-3:2011; electrically propelled road vehicles, safety specifications part 3 [15]: protection of persons against electric shock.

In addition, **ISO 15118** "Road Vehicles – vehicle to grid communication interface", specifies the communication between Electric Vehicles (EV) and power supply equipment. Useful indications about test methods for evaluating automotive EMC issues are also provided by **ISO 11451 and ISO 1145**.

5.1 Reference documents

Along with the list above, reference documents supporting the regulatory framework for wireless charging of electric vehicles are:

1. **SAE J2954 recommended practice** [1]**:** "Wireless power transfer for light-duty plug-in/electric vehicles and alignment methodology" (2017, updated in 2019).
2. **ISO/PAS 19363 published document** [16]**:** "Electrically propelled road vehicles, magnetic field wireless power transfer safety and interoperability requirements" (2017, updated 2020).
3. **IEC 61980 International Standard** [2-4]**:** "Electric vehicle wireless power transfer (WPT) systems". Part 1: General requirements (International Standard). Part 3: Specific requirements for the magnetic field WPT systems (Technical Specification) (2015).

The covers of these three documents are shown in Figure 4.

SAE J2954 recommended practice *ISO/PAS 19363 published doc* *IEC 61980 International Standard*

Figure 4. Covers of the three main documents related to the wireless charging of electric vehicles.

The scope and emphasis of these Standards are slightly different from those of the list above:

1. The scope of SAE J2954 is to define an "*industry wide specification that defines acceptable criteria for interoperability, electromagnetic compatibility, EMF* [exposure]*, minimum performance, safety and testing for wireless charging of light duty electric and plug-in electric vehicles*". It is intended for stationary applications, when the vehicle is parked, and for above ground surface transmitter assembly.
2. The scope of ISO/PAS 19363 is to provide "… *requirements and operation of the on-board vehicle equipment that enables magnetic field wireless power transfer (MF-WPT) for traction battery charging of electric vehicles. It is intended to be used for passenger cars and light duty vehicles"*. The document addresses the following issues:
    - transferred power;
    - ground clearance;
    - interoperability requirements;
    - performance requirements under various conditions;
    - safety requirements;
    - test procedures.
3. Documents IEC 61980-1 and 61980-3 deal with "*equipment for the wireless power transfer of electric power from the supply network to electric road vehicles… at standard supply voltages ratings… up to 1000 V AC and up to 1500 V DC"*. Several aspects are covered, in particular:

- characteristics and operating conditions;
- specification for required level of electrical safety;
- requirements for basic communication for safety and process matters;
- requirements for basic positioning, efficiency and process matters;
- specific EMC requirements for WPT systems.

In the following subsections the main requirements are highlighted and discussed.

5.2 Reference coordinate system

In order to provide well defined vehicle locations, the three documents provide a reference coordinate system. They all set the Z-axis in the vertical orientation with Z = 0 m at ground level, where the X-Y plane is the ground plane. The origin of the coordinate system is the geometric centre of the GA coil (or primary coil). Both for SAE J2954 and ISO/PAS 19363 the X-axis is opposite to the direction of motion, whereas for IEC 61980 the X-axis is oriented in the direction of the vehicle motion (see Figure 5).

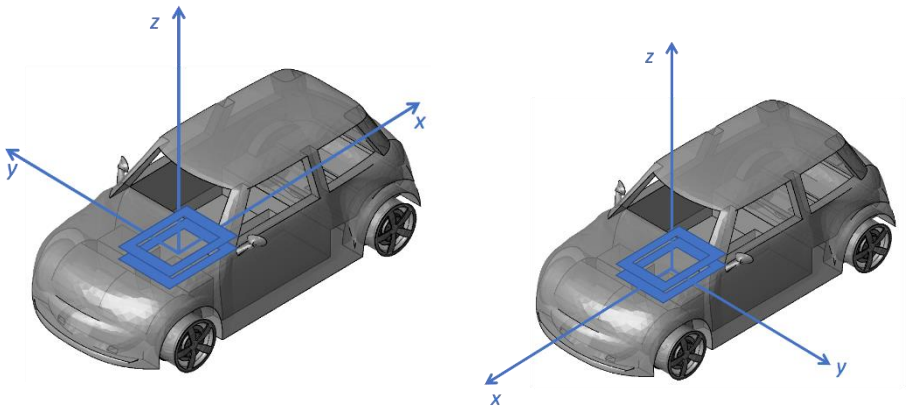

a) SAE J2954 and ISO/PAS 19363 b) IEC 61980

Figure 5. Reference coordinate system from different standards.

5.3 Classification of WPT systems

The main classification of WPT systems is based on the input power, which is the maximum power drawn from the grid. All Standards introduce four classes, from WPT1 to WPT4. The IEC 61980 also introduces an additional class WPT5 for heavy duty vehicles, as shown in Table 1. Note that ISO/PAS 19363 refers to the IEC 61980 power classes.

Table 1. Input power classes. SAE J2954 defines the WPT classes in terms of volt-ampere.

	WPT1	**WPT2**	**WPT3**	**WPT4**	**WPT5**
Maximum input power	3.7 kW	7.7 kW	11.1 kW	22 kW	>22kW

For each class the minimum power transfer efficiency at nominal alignment along with maximum misalignment is also reported. WPT4 and WPT5 are currently under consideration for future editions.

The maximum misalignment allowed in the X-Y plane is X = 75 mm, Y = 100 mm. For the misalignment along the Z-axis, the efficiency must be guaranteed for the whole Z-plane variation allowed: Z = [Z_{min}, Z_{max}] (*see Table 2*).

Another classification is based on the allowed clearance between the ground side and vehicle side. Three dimensions can be considered for this purpose as shown in Figure 6:

A. "magnetic air gap" (SAE J2954) or "operational air gap" (IEC 61980);
B. "mechanical air gap" (IEC 61980);
C. "VA coil ground clearance" (SAE J2954) or "secondary device ground clearance" (IEC 61980 and ISO/PAS 19363).

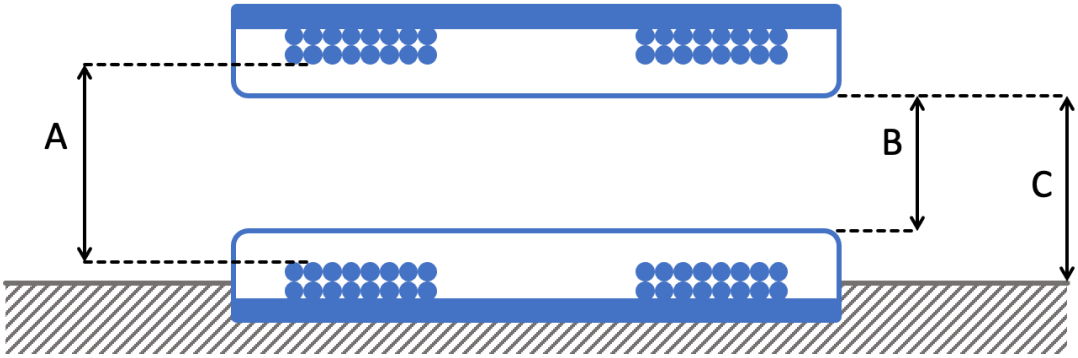

Figure 6. Physical dimensions along Z-axis.

The Z-class refers to the ground clearance, indicated by C in Figure 6, and the classification range is reported in Table 2.

Table 2. Z-class classification.

Z-class	Ground clearance range
Z1	100 mm – 150 mm
Z2	140 mm – 210 mm
Z3	170 mm – 250 mm

6. Magnetic field exposure limits for human beings

6.1 Exposure limits

The limits of human exposure to emissions from electromagnetic systems are defined by numerous international and national standards, guidelines and regulations. It is not possible, and perhaps not even useful, to summarise them all in this document, therefore this guide summarises the most relevant and makes reference to the International Commission on Non-Ionizing Radiation Protection (ICNIRP 2010) guidelines.

The legislation often distinguishes between exposure for the general public and occupational exposure. The exposure limits for the general public employ a conservative approach.

In the following sections, the limits in terms of basic restrictions and reference levels follow ICNIRP 2010 requirements. Limits concerning EMF (both reference levels and basic restrictions) and contact currents (reference levels) are reported in Appendix B.

ICNIRP Guidelines 2010
ICNIRP 2010 [17] "Guidelines for limiting exposure to time-varying electric and magnetic fields (1 Hz to 100 kHz)".

The limits introduced by ICNIRP are based on established evidence regarding acute effects. Currently, available knowledge indicates that adherence to such restrictions protect human beings from adverse health effects from exposure to low frequency EMF, and the ICNIRP guidelines outline what these acute effects are. The ICNIRP guidelines introduce two types of limits, (1) basic restrictions and (2) reference levels. Reference levels are defined both for EMF exposure and for contact currents.

- **Basic restrictions (BR)**: in the ICNIRP guidelines, the physical quantity used to specify the basic restrictions on exposure to EMF is the internal electric field strength E_i, as it is the electric field that affects nerve cells and other electrically sensitive cells. E_i is not trivial to calculate as it requires complex dosimetric models; therefore, the reference levels are introduced.
- **Reference levels (RL)**: RLs are given in terms of measurable electric and magnetic fields (specifically magnetic flux density) in air. RLs have been determined by mathematical modelling for the exposure conditions where the variation of the electric or magnetic field over the space occupied by the body is relatively small, i.e., uniform exposures.
- **Reference levels for contact current** up to 10 MHz are also provided to avoid shock and burn hazards.

Compliance with RLs should guarantee compliance with BRs, while the opposite is not guaranteed. This is valid in general, provided that the absolute maximum value of EMF is correctly detected and compared with the corresponding RL. In the case of strongly heterogeneous fields (e.g. gradient fields of a MRI system), this is not an easy task. For example, an experimental assessment may only provide field averages over a certain area, due to the finite size of the magnetic field probe used to perform the measurements. If the maximum field value is (even slightly) underestimated, compliance may be achieved with respect to the RLs, whereas a dosimetric assessment in terms of induced electric field may reveal that the latter does not comply with the BRs.

ICNIRP Guidelines 1998
ICNIRP 1998 [18] "ICNIRP guidelines for limiting exposure to time-varying electric, magnetic and electromagnetic fields (up to 300 GHz)". These guidelines are still used even though they have been replaced by ICNIRP Guidelines 2010 for the frequencies of interest for WPT

charging of vehicles, and they have been replaced by ICNIRP Guidelines 2020 for frequencies above 100 kHz.

ICNIRP Guidelines 2020
ICNIRP Guidelines for Limiting Exposure to Electromagnetic Fields (100 kHz to 300 GHz), i.e. radio frequency [19]. In the case of static inductive charging of electric vehicles at 85 kHz, no significant harmonics of the magnetic field were highlighted and no harmonics above 100 kHz were observed with significant amplitude to justify an evaluation of the specific absorption rate (SAR).

European directive 2013/35/EU
The directive concerns the minimum health and safety requirements regarding the exposure of workers to the risks arising from electromagnetic fields. Like ICNIRP, the directive covers only scientifically well-established links between short-term direct biophysical effects and exposure to electromagnetic fields and it does not cover hypothetical long-term effects.
The limits suggested by the European directive are similar to those indicated by ICNIRP for occupational exposure, but there is a difference in terminology as shown in Table 3.

Table 3. Correlation between ICNIRP and 2013/35/EU limits.

ICNIRP 2010	***EU DIRECTIVE 2013/35***
Basic restrictions (both EMF and contact currents)	Exposure limit values
Reference levels	Action levels

European Recommendation 1999/519/EC
The EU recommendation "on the limitation of exposure of the general public to EMF (0 hertz to 300 gigahertz)". The limits of the recommendation are derived from the 1998 ICNIRP guidelines. The terminology in this document is consistent with directive 2013/35/EU.

IEEE Std C95.1™-2019
This standard [20] concerns safety levels with respect to human exposure to electric, magnetic, and electromagnetic field limits. The frequency range is between 0 Hz to 300 GHz and includes the frequency bandwidth of interest for WPT charging of vehicles, of up to 100 kHz. The limits, which incorporate safety margins, are expressed in terms of dosimetric reference limits (DRL), which correspond to ICNIRP basic restrictions, and exposure reference levels (ERL), which in turn correspond to ICNIRP reference levels. Despite the correlation, the IEEE and ICNIRP limits are quite different.

The EMF policy differs in different countries around the world, including within Europe. Since the EU recommendation is not legally binding, EMF policy is different in different member states. An overview of the world situation is provided by [21].

Regarding the three documents in Section 5.1, relating to human exposure to electromagnetic fields generated by the transmission system, SAE J2954 Recommended Practice, ISO/PAS 19363 Published Document and IEC 61980 International Standard refer to the following standards:

- IEC 61980: Depending on national or local regulations, reference is made to the ICNIRP Guidelines 1998 or 2010. The EMF exposure specifications are reported in the informative Annex C;
- ISO/PAS 19363: ICNIRP Guidelines 2010 (1998 only if required by regional regulations);
- SAE J2954: ICNIRP 2010, taking peak values as reference.

Exposure measurements are outlined in Section 7, and Appendix C summarises and compares the main procedures described in IEC 61980 and ISO/PAS 19363 in order to protect humans against deleterious electromagnetic effects.

6.2 Implanted medical devices

Implanted medical devices (IMD) and active IMD (AIMD), including but not limited to pacemakers, defibrillators, neurostimulators and infusion pumps, require specific consideration.

Any emission from an emitter that exceeds the ICNIRP 1998 limits would be a potential source of interference to AIMD. Adoption of higher emission levels may expose patients to unnecessary risk. However, for AIMDs, more restrictive reference levels are formulated by ISO 14117 standard [22] and are adopted by SAE J2954 standard [1]. The limits are specified in Appendix M of [22] where a chart is provided for pacemakers and implantable cardioverter defibrillators. The chart shows the magnetic field limits (peaks) for AIMD and specifies four regions: 1) sensing and operation region; 2) operation unaffected region; 3) no permanent damage or operation unknown, no permanent malfunction region and finally 4) operation unknown or permanent damage possible region.

It requires caution to operate in region 2 specified above, where in the frequency range of interest between 10 kHz and 100 kHz, the limits correspond to a level of magnetic flux density in air (peak) ≤ 15 μT. This limit has to be verified inside and around the vehicle, but, of course, not necessarily below the vehicle. SAE J2954 suggests that verification of such a limit is carried out by using a common 100 cm^2 standard field probe. If a measurement point shows a reading above 15.0 μT, [1] suggests that the average of four measurements made in a 2 x 2 grid, spaced by 7.5 cm with the probe centred at each point is taken.

Section 8.2.7, below, summarises the main steps of a procedure for the safety assessment of conductive medical implants through a hybrid modelling approach.

7. Exposure measurements

7.1 Introduction to exposure measurements

Exposure measurements around WPT systems require significant preparation, which includes setting up the measurement site and identifying the measurement locations. Firstly, the transmitter and receiver coil need to be aligned or deliberately misaligned by a required displacement value that should be precisely measured. All measurement instrumentation should be selected based on its specification and performance and calibrated at the appropriate points of use. This should include suitable transducers that need to be installed as part of the coil current measurement system (see Section 7.1.4). The locations of each measurement point need to be accurately determined with respect to a reference coordinate system. The magnetic field measurements should be synchronised with the measurements of the coil currents, to ensure that the current value at each time instant is known throughout the whole duration of the exposure measurements.

The following subsections detail the various phases of the exposure measurements.

7.1.1 Setting up the measurement site

Prior to the start of human exposure measurements, one needs to define what the measurement system should analyse. The following definitions are given:

- Board assembly: BA, as defined in Section 4, including the Rx coil.
- Ground assembly: GA, as defined in Section 4, including the Tx coil and the load (batteries or equivalent load).
- Vehicle-body: is the vehicle chassis part of the BA, at the bottom of which the Rx system is located.

The GA, BA and vehicle body taken together are referred to as the WPT assembly.

The WPT assembly must be located in a measurement site far from significant metallic objects (conductive and/or ferromagnetic) that may perturb the magnetic field, thus leading to inaccurate measurement results.

7.1.2 Coil alignment

The magnetic field emitted around the Rx-Tx coils of a WPT assembly is dependent on the coil alignment/misalignment. For a given system architecture, which includes magnetic flux concentrators as well as shielding, the minimum field is obtained when the coils are aligned. Measurement repeatability is strictly linked to the alignment repeatability. Therefore, a measurement procedure is required, allowing the determination of a geometrical parameter (e.g. a coordinate pair) which can be associated to the measurements. Various systems are available for the measurement of the coil alignment, and this guide covers those making use of triangulation methods (Section 7.1.5) and magnetic sensors. SAE J2594 can be used for more details on alignment procedures.

In these guidelines, the Rx-Tx coil positions are considered as an intrinsic parameter of the charging system and it will not be included in the measurement uncertainty calculations.

7.1.3 Choice and calibration of AC magnetic field meters

AC magnetic field meters need to provide the resultant of the magnetic induction (r.m.s. or peak) at a point. The commercially available instruments can be broadly divided into two categories:

- Induction probes (including a sensing coil);
- Hall probes.

Depending upon the frequency of operation, individual instrument specifications should be evaluated and calibrated at the appropriate field and frequency levels. The preferred choice is for the use of three axis probes, which can measure each axis component at the same time. Where uniaxial sensors are used, they should be centred at the measurement location and three sequential measurements made when aligned along the direction of three orthogonal (X, Y and Z) axes.

The larger the sensor area, the smaller the uncertainty contribution for probe positioning, which leads to a greater signal-to-noise ratio. However, the averaging effect has a stronger influence on the uncertainty calculation [23].
Concerning the operational frequency range of the selected magnetic field probe, the currents in the resonant circuit of the WPT assembly are sinusoidal waveforms with a small distortion reported at the third and fifth harmonics [24]. Therefore, the instrument's frequency bandwidth should be at least > 3 f and ideally > 5 f, where f is the wireless transmission frequency.

7.1.4 Coil current measurements

Measurements of the magnetic field in air need to be correlated to the field sources (i.e. resonant coils) current signal magnitude. This is useful when the human exposure measurements are associated with predictive models (Section 8) that are used for comparison purposes, in addition to experimental results. Predictive models are built upon the geometry of the WPT assembly. In the simulation model, the current through the Tx and Rx coils should be assigned the values measured on-site. The following steps should be followed to ensure that magnetic field measurements in air are correlated to current measurements:

- The field measurement needs to be acquired at a known time. For this purpose, a data acquisition card (DAQ) may be connected to the AC magnetic field meter. In this case, the meter's output should either have no time delay or a known delay to be corrected for (e.g. analogue output).
- Current transducers should be calibrated prior to measurements and have a high frequency range of at least 10 times the measurement frequency, to minimise phase angle errors. For the reasons mentioned above, the two transducers should be identical and have an analogue output.
- The Tx and Rx currents should be measured simultaneously and synchronised with the field measurements. If cables are long enough, a single DAQ may be used; alternatively, one could use a multi-channel oscilloscope with negligible channel-to-channel skew at the WPT resonant frequency. For example, if the resonant frequency is 85 kHz, a 1-degree phase angle corresponds to 33 ns, and the channel-to-channel skew should be at least one order of magnitude lower than this value. This enables the reconstruction of the relations between current phases that are required for the use of mathematical models. If the distance between the current transducers prevents the use of a single DAQ, synchronised systems should be used instead.

7.1.5 Positioning of the AC magnetic field meter

The AC magnetic field meters need to be accurately positioned in locations corresponding to the measurement points. This can be done manually, by using visual references, placed on the ground and measuring their distances to other objects using distance measuring instruments. More advanced methods involve the use of a triangulation system based on optical sensors or cameras enabling reconstruction of the probe location in a 2D or 3D space. This requires firstly, attaching two static tracking targets onto accurately known locations and, secondly, attaching a target to the probe's head. Provided that the two static targets and the probe's head target are visible, the tracking system can be moved arbitrarily and the software reading the target locations can calculate the global position by using basic rotational matrices. An example of such systems is given in [25].

7.1.6 Measuring the magnetic field

Prior to exposure measurements, a measurement of the background ambient field must be performed. All the electronic equipment located in the area surrounding the WPT may be switched on, but no electric current should be flowing in the inductive charging system, which should be off. This measurement allows a determination of which areas in and around the charging system have negligible or non-negligible impact on the field levels.
Throughout the measurements, synchronization with current measurements should be in place, as explained in Section 7.1.4.
Determination of the exposure inside and around the vehicle occurs by placing the measurement point inside the vehicle body and around it, respectively. We can distinguish between two cases:

1. Light vehicles (e.g. cars) and
2. Heavy vehicles (e.g. trucks and buses).

1. Light vehicles

The position of passengers and bystanders in and around a light vehicle are represented in Figure 7.

Passengers

The locations where the field measurements should be performed are identified by the locations of: 1) the driver, 2) the passenger in the rear middle seat, and 3) the passenger in a side rear seat (assuming symmetric magnetic field distributions on the two sides of the vehicle) (Figure 7 a). For each of these, the field should be measured in three locations:

- At the vehicle ground level, in the proximity of the passenger's ankles;
- At a height equal to half of the seated passenger's height;
- At the headrest height.

Bystanders

Three positions of the Rx coil are considered for the evaluation of the bystanders' exposure (Figure 7 b):

- Coil under the front part of the vehicle (C1);
- Coil under the central part of the vehicle (C2);
- Coil under the rear part of the vehicle (C3).

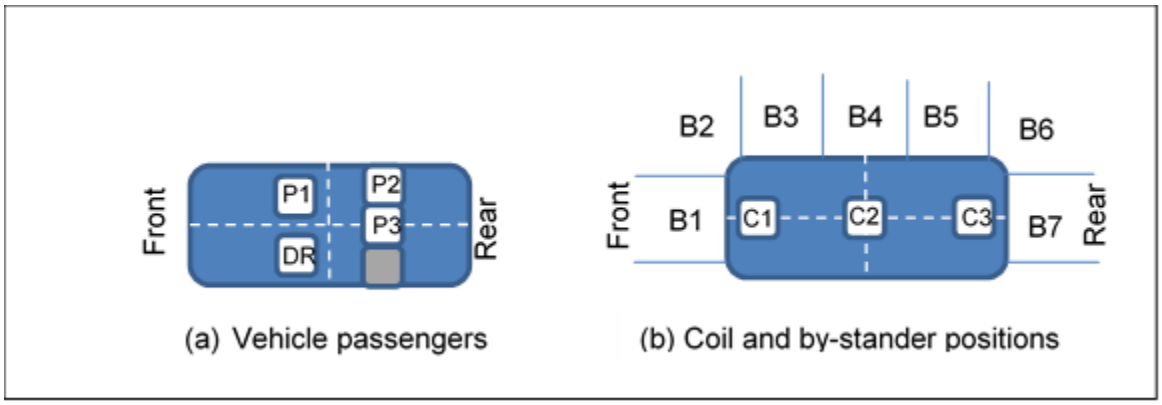

Figure 7. Positions of passengers and bystanders.

In order to minimise the number of measurements required for the exposure assessment in the scenarios identified in Figure 7, the choice of locations where the magnetic field should be measured can be made such that it provides an indication of the maximum field levels. Since the magnetic field is maximum at lower distances from the transmitter coil, the following measurement protocol can be established for each of the three coil locations:

- C1: the exposure of the bystanders that are closer to the coil may be evaluated (i.e. B1, B2 and B3);
- C2: the exposure of B3, B4 and B5 may be assessed;
- C3: only B5, B6 and B7 are included in the exposure measurement.

The exposure assessment for each position where the magnetic flux density is measured, B1-B7, is evaluated using four measurements, at the following heights (along the Z-axis), each of which corresponds to a part of the body:

1. Z = 0.1 m (ankle)
2. Z = 0.5 m (knee)
3. Z = 1.4 m (trunk)
4. Z = 1.7 m (head)

2. Heavy vehicles

The same method as the one described for light vehicles may be adopted for trucks or vans and, more broadly, heavy vehicles. The two cases of trucks and buses are slightly different from each other, as buses have an entrance door and passengers accessing them should be taken into account. On the other hand, the only person contributing to the exposure measurement in trucks is the driver and the exposure scenario can be limited to his/her position. For example, to determine the exposure inside and around a bus, the following measurement points should be considered:

- A bystander approaching the bus entrance;
- Two bystanders in an area close to the Rx coil (same as Figure 7);
- Two bus passengers located inside the bus, either above the Rx coil (if possible, if the area is accessible to passengers), or close to the receiving coil (driver).

In summary, the exposure of the driver and of five passengers must be considered.

Measurements need to be performed at a height representative of the human body exposure. The following heights from the ground are considered for bystanders:

- Z=0.1 m (ankle);
- Z=0.5 m (knee);
- Z=1.4 m (trunk);
- Z=1.7 m (head).

For the bus passengers, these heights are also relevant, but they are measured from the bus floor rather than the ground level.

The driver exposure may be evaluated with measurements on the spot, in the following positions:

- On the vehicle ground level, in proximity of the passengers' ankles;
- At a height equal to half of the passengers' seated height;
- At the headrest height.

7.1.7 Probe averaging effect

The measurement of AC magnetic fields is usually performed with a magnetic field probe containing three concentric coils, each with a known area (see Section 7.1.3). The measured field is the square root of the sum of the squares of the three orthogonal concentric coils. In a uniform spatial magnetic field, the magnetic field at the centre of the probe is the same as the average value measured by the probe. However, in a non-uniform spatial magnetic field, the magnetic field at the centre of each coil may differ from the average value measured by the same coil. This effect may be larger as the area of the coils becomes larger, especially in highly divergent fields, which is the case with WPT charging stations.

Simulations to determine the spatial uncertainty accounting for the probe volume

The spatial uncertainty accounting for the probe volume may be estimated from simulations of the magnetic field performed using a software tool for electromagnetic computations (Section 8.1), by considering all desired probe positions, inside and outside the vehicle, and calculating the relative uncertainty of the computed values, in the following way.

- For each probe position, a cubical magnetic field probe is chosen with dimensions such that it fits inside the spherical probe used in the field measurements and can thus account for the behaviour highlighted by the measurements.
- The magnetic field in the cubical probe is sampled at a number of equally- spaced points (e.g. 1 cm apart). For each of these points, the average of the magnetic field for the cubical probe and the magnetic field value at the centre of the probe is calculated.

The mean relative uncertainty for the magnetic field is calculated by comparing 1) the mean B-field for the cubical probe and 2) the B-field at the centre point of the probe.

To simulate an isotropic probe, it is not mandatory to use the cubic shape. One can also use a spherical shape, which is even more realistic. However, the cubic shape simplifies the work required to numerically analyse a matrix of points in the volume concerned and provides a comparable accuracy.

7.2 Measurement results

7.2.1 Presentation of the measurement results

The measurement results should include, for each measurement point:

- the resultant magnetic field (or magnetic flux density);
- the coordinates of the measurement point, with respect to a known reference system (e.g. the geometric centre of one of the Tx and Rx coils);
- an indication of whether the measurement point is referenced to the position of a passenger or bystander and of its height from either the vehicle floor or ground depending on whether the measurement refers to a passenger or bystander;
- the Tx and Rx coil currents;
- the relative position of the coils;
- measurement date and time.

The measurement uncertainty also needs to be stated, as detailed in Section 7.2.2.
Additional data that may be included are:

- the magnetic flux density (or magnetic field strength) components along the X, Y and Z directions, read from the AC field meter and referred to the chosen reference system;
- the phase relationship between the Tx and Rx currents, if the measurement is to be used as an input for a numerical model;
- photographic record (if available).

Measurements may be reported in a table as shown in Table 4.

Table 4. Example of how to record a set of measurement data.

Date: …….	COIL alignment (m) [(0,0 for centered coils, otherwise specify misalignment) (X, Y)	Background field: …….. µT

ID	Time and meas. filename (if any) (e.g. GPS time trigger)	Location	Photo (Ref if any)	Tx current r.m.s. (A)	Rx current r.m.s. (A)	Currents Phase shift	Measurement position (m) X Y Z	Magnetic flux density B [T]
1	dd.mm.yy hh.mm.ss filename	(e.g.) Knee B1	(e.g. DSC_0)	….	…..	……		

7.2.2 Uncertainty analysis of the measurement results

Uncertainty assessment relies on international guidelines and methods [26]. The terminology used in this section is derived from [26]. The methods that can be used for uncertainty calculation are based on separating the total uncertainty budget into several quantifiable components that are uncorrelated or with limited interdependency, determining the uncertainty contribution using assumed statistical models and calculating the total uncertainty as a root-sum-square (RSS) value. In accordance with [26], effective degrees of freedom apply to statistically derived uncertainties for which the sample sizes are used to determine the coverage factor; they are assumed to be infinite for all Type B evaluations.

Throughout the analysis proposed here, all uncertainty components were assessed using Type B evaluation, hence the degrees of freedom were taken to be infinite. Each uncertainty source listed below is shown in the format: “uncertainty source: description of each uncertainty component”.

- Tolerance in dB: the tolerance of each component, expressed in dB in terms of its influence on the quantity of interest;
- probability distribution: the variation in probability of the true value lying at any particular offset from the measured result (either normal or rectangular);

- divisor: typically equal to 2 for a normal distribution or $\sqrt{3}$ (1.7321) for a rectangular distribution;
- sensitivity coefficient: the sensitivity coefficient of each uncertainty component that translates the unit of the tolerance to the unit for which the uncertainty is determined. In this case, all tolerances are already expressed in dB relative to the quantity of interest, the sensitivity coefficient is unity for all contributing components and estimated to be negligible for non-significant contributions.
- standard uncertainty in dB: the contribution of the uncertainty component to the combined standard uncertainty.

The terms considered to obtain expanded uncertainties (k = 2.95 % coverage factor) are:

- U_m: relates to the magnetic field (magnetic flux density) meter calibration. U_m can be a function of a specific measurement range.
- U_t: relates to the positioning accuracy (see Section 7.2.2.1).
- U_s: the spatial uncertainty accounting for the averaging effect of the B-field probe can be estimated according to Section 7.1.3;
- U_r: the uncertainty related to reproducibility (repeatability of the measurement).

Table 5 shows an example of an uncertainty budget.

Table 5 – Typical uncertainty budget for magnetic field measurements. Quantities in the last column are derived from U_s by using the table.

Source of Uncertainty	Value	Probability	Divisor	c_1	u_1
	%	Distribution			%
Calibration of the field meter	U_m	Normal	2	1	u_m
Tracker positional accuracy (automated) Or manual positioning accuracy	U_t	Rectangular	1.7321	1	u_t
Spatial uncertainty accounting for probe volume	U_s	Normal	2	1	u_s
Reproducibility	U_r	Normal	2	1	u_r
Combined uncertainty for 3D tracked measurements		**Normal**			u_{tot}
Expanded uncertainty for 3D tracked measurements		**Normal**	**k = 2**		U_{tot}

7.2.2.1 Uncertainty of the meter positioning system

The method to estimate the uncertainty of the meter positioning system depends on the type of system that is used. As an example, systems based on optical cameras may be chosen as discussed in Section 7.1.5. These systems can be used to track the position of an object which is moved in a 2D space, by placing it on a robotic arm. The uncertainty evaluation of the object's position will need to incorporate all relevant factors, including the uncertainty introduced by transformations from local coordinates to global coordinates. Once the coordinates are expressed with respect to the global coordinate system, the coordinate measurement uncertainty can be determined by calculating the root mean square (RMS) of the contributions that are listed in Table 6.

Table 6 – Typical uncertainty budget for an optical positioning system.

Source of Uncertainty	Value	Probability	Divisor	c_1	u_1
	%				%
Coordinate transformation	U_c	Rectangular	1.7321	1	u_c
Robotic arm	U_r	Rectangular	1.7321	1	u_r
Coordinate measurement	U_m	Normal	2	1	u_m
Combined uncertainty for 3D tracked measurements		**Normal**	***k* = 2**		$\boldsymbol{u_{tot}}$
Expanded uncertainty for 3D tracked measurements		**Normal**	***k* = 2**		$\boldsymbol{U_{tot}}$

7.2.2.2 AC field meter calibration

Various National Metrology Institutes (NMIs) and calibration laboratories have the capability to characterise AC magnetic field meters at the field levels and frequencies of interest. A list of NMIs with this capability is given in Appendix F.

To conduct AC magnetic field measurements on these types of instruments and to achieve the lowest uncertainties, a number of basic requirements need to be satisfied:

- An environment with minimal AC magnetic field background;
- A stable field generating source, such as Helmholtz coils with good temperature stability and minimal long-term drift;
- A field generating source of sufficient size such that field uniformity does not impact the measurement uncertainty;
- Other equipment used, such as current shunts to measure current, should be characterised at the frequencies of interest.

Helmholtz coils

Helmholtz coils are used to generate a uniform region of magnetic field along the axis of the coil. When the separation, s, of two identical coils is equal to the radius r, the Helmholtz condition is satisfied. A typical arrangement is shown in Figure 8 where:

s is the separation between coil 1 and coil 2;
r is the coil radius;
a is the distance from each coil to the mid-plane, a = s/2.

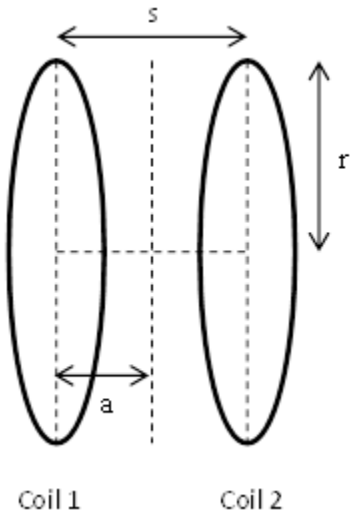

Figure 8. The arrangement of Helmholtz coils.

For the lowest uncertainty, the coil constant, defined as the ratio of the magnetic field strength to the current in the coils, is determined at DC using a proton resonance method. The required field strength is then established by calculating the current needed to generate the field, and measuring the current using a calibrated resistor and calibrated digital voltmeter (DVM).

The accuracy of the magnetic fields produced within Helmholtz coils is primarily affected by the accuracy with which they are constructed, and the accuracy with which the current driving them is known. The coil constant of Helmholtz coils, in A/m/A, is given by the relationship:

$$\frac{H}{I} = \frac{8}{5\sqrt{5}}\frac{N}{r} \qquad (1)$$

here

H is the axial magnetic field strength, in A/m;
I is the current in the coils, in A;
N is the number of turns on each coil;
r is the radius of each coil, in m.

For the DC determination of the coil constant, the traceability to the SI is obtained via frequency (related to the output of the proton resonance magnetometer) for the magnetic field measurement and to DC resistance (calibrated standard resistor) and voltage (calibrated DVM) for the current measurement. For the AC determination, the change in coil constant with increasing frequency (or frequency dependence) can be assessed using a single turn search coil. The single turn search coil should have no significant frequency dependency in the frequency range considered, and the change in coil constant is determined with respect to the DC value. AC traceability to the SI is obtained via AC/DC transfer standards for AC resistance (calibrated shunts) and voltage (calibrated DVMs).

For single axis or for individual axes of three-axis instruments, the sensor of the field meter to be calibrated should be positioned coaxially midway between the two Helmholtz coils. The sensor is then aligned so it is measuring the maximum magnetic flux density, by monitoring its displayed reading or output voltage (depending upon the instrument) while the sensor is moved in-plane by controlled rotation around its central axis. At the required magnetic field strength, the output reading of the field meter is recorded. If the sensor output is an analogue voltage, a calibrated DVM is used. The voltage measured across a calibrated resistor is

recorded and used to determine the coil current and the magnetic field can be determined from the coil constant.

If the resultant measured output from a three-axis instrument is required, the sensor can be aligned so that the magnetic flux density measured by each of the three sensor coils is approximately equal.

Following the calibration of the field meters the measurement uncertainty is calculated by assessing all relevant contributions that could affect the final measurement result.

The main uncertainty contributions for the measurement include, but may not be limited to:

- coil constant uncertainty;
- alignment of sensor – to confirm that the maximum field is being measured;
- non-uniformity of field – determined for the sensor calibrated during the measurement;
- equipment used to measure current:
    - calibrated resistor, including error from nominal value, uncertainty and frequency dependence;
    - DVMs, including error from nominal value, uncertainty and linearity;
- measurement of frequency;
- repeatability.

Depending upon the size of the Helmholtz coils of the sensor under test, the non-uniformity of the field may be one of the most significant contributions. The percentage uncertainty contribution due to field non-uniformity of an ideal Helmholtz coil can be estimated from Figure 9 and Figure 10 which are plots of the coil constant against the ratio of the radius of the sensor and the distance along the axis to the radius of the coils, respectively.

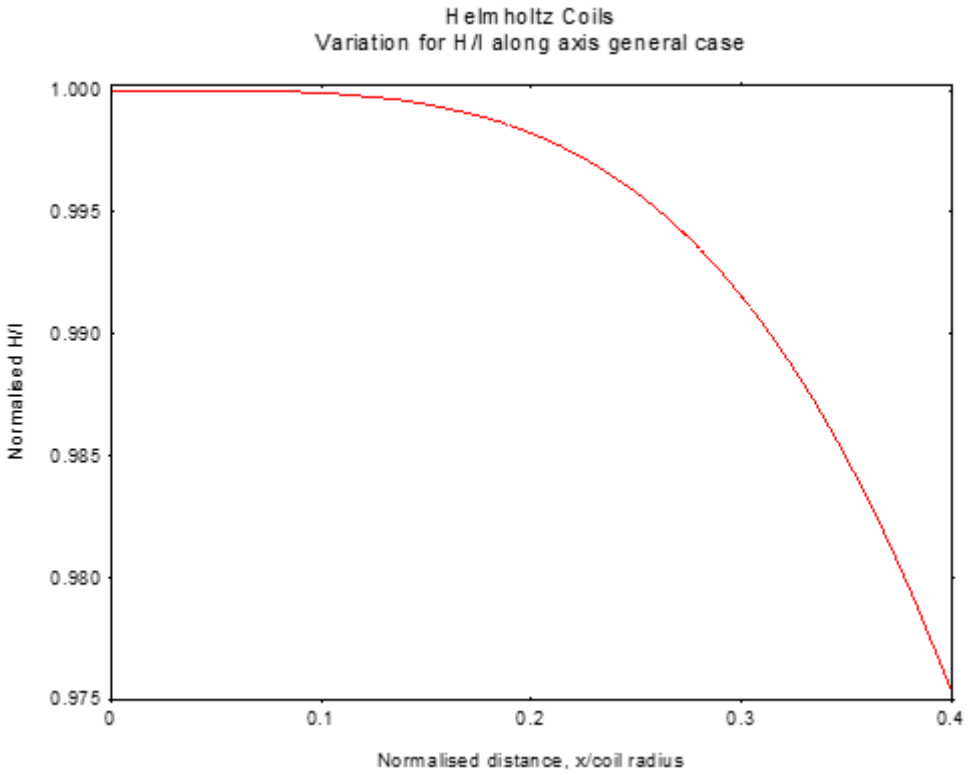

Figure 9. Variation of H/I along the X-axis (axis through the centre) of the coils.

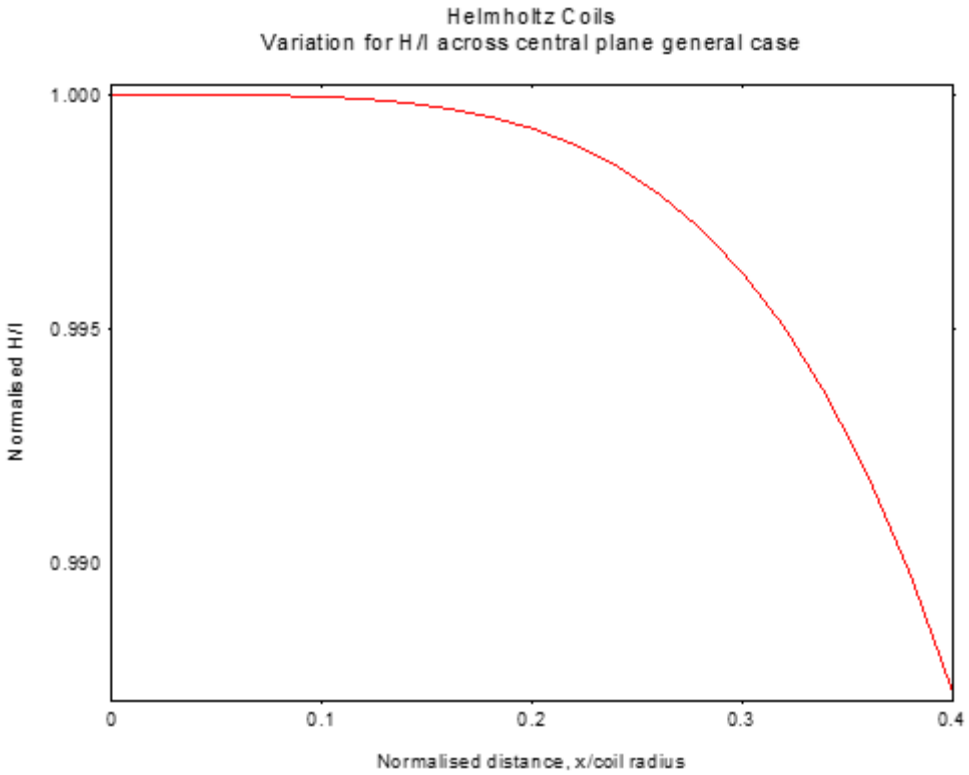

Figure 10. Variation of H/I across the central plane (X = 0) between the coils.

To correct for the effects of finite width of coil windings, the uniformity can be improved by adjusting the spacing. Alternative coil arrangements that provide more homogeneous field regions like compensated coils can also be used.

7.3 Limb current measurements

Limb current clamps usually consist of a toroidal coil that can be placed around the ankle or arm and are usually connected to a meter unit or computer to record the induced current. They can be used to assess human exposure to EMF over a broad frequency range allowing a comparison against stated reference limits for induced limb current that are given by the International Commission on Non-Ionizing Radiation Protection (ICNIRP, see Section 6).

It is important that these clamps are calibrated accurately at the current levels and frequencies of interest and that the calibrations are traceable to National Standards. Various techniques are employed to carry out the calibration of these types of device, including rod antenna systems located in GTEM cells, or the use of a coaxial line that the clamp can be centred around.

Commercial instruments can operate from a few kHz up to more than 100 MHz, where the clamp sensor is commonly a split ferrite core transformer allowing for ease of positioning. Some manufacturers use optical fibre coupled meter units to limit perturbation of the measured RF field or current distributions.

Table B2 in Appendix B outlines the ICNIRP [17,18] reference levels for contact and induced currents. The physical areas that require to be addressed are those that are likely to be close to the WPT systems, e.g. the ankles, where the maxima magnetic fields are observed.

8. Calculation of the exposure

Human exposure assessment can take place on an existing system or on the design of a system. In the first case, the calculation may be necessary to assess situations that could introduce exposure risks, as reported in Figure 11. In the second case, the calculation is necessary to evaluate the compliance of the emissions with human exposure *a priori* (Figure 12).

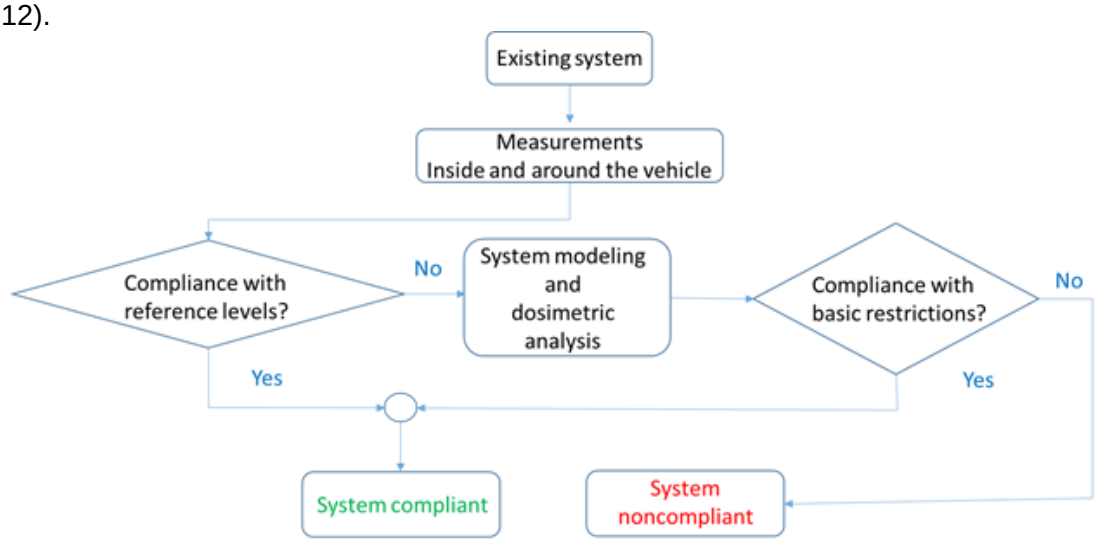

Figure 11. Evaluation of the compliance with the human exposure to magnetic fields of an existing system.

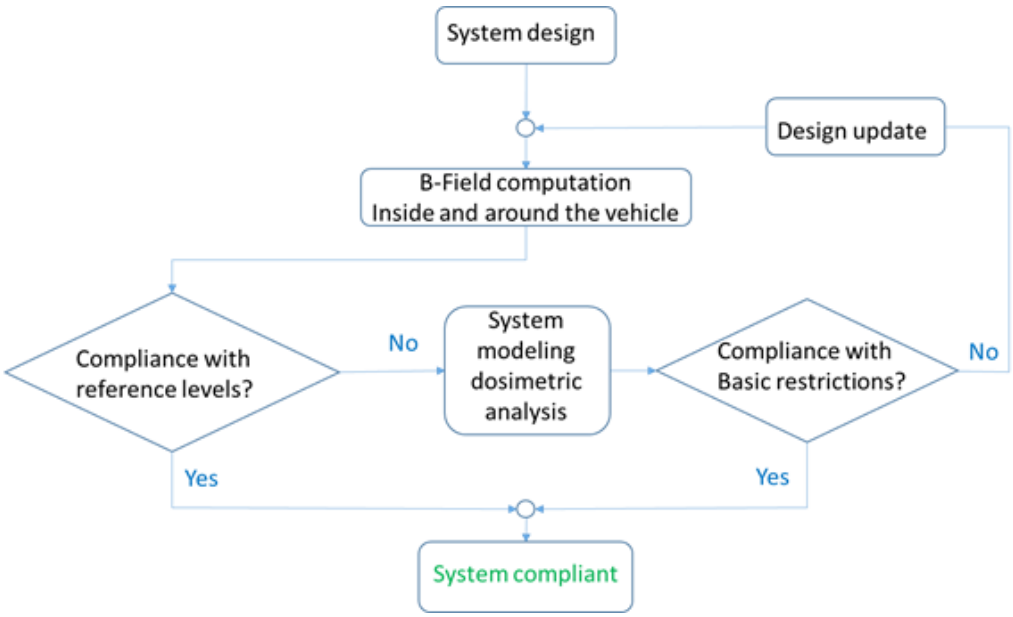

Figure 12. Evaluation of the compliance with the human exposure to magnetic fields of a system under design.

The calculation must include the assessment of the levels of magnetic fields inside and around the vehicle. If the latter exceeds the reference levels (Section 6), such calculation can also be used for a dosimetric evaluation to verify the basic restrictions, which normally start from the magnetic field values calculated in air, assuming that the currents induced in the human body do not significantly disturb the field generated by the inductive charging system. Dosimetric evaluation is discussed in Section 8.2.

8.1 Computation of the magnetic field levels at the charging station and inside the vehicle

The calculation of magnetic induction levels around and inside a vehicle can be carried out with a range of numerical approaches [27], [28], [29], [30], [31]. A list of the most popular computational methods follows.

1. Finite element method (FEM) [27], [28]

The finite element method is based on the solution of Maxwell Equations in their differential form.

The method is based on the approximation of the solution by means of the superposition of reconstructors having a simple analytical expression. By approximating the exact solution with a superposition of simple analytical functions, the differential operators can be computed explicitly, leading to the definition of a matrix of algebraic equations. In order to apply this approach, FEM requires the subdivision of the domain into a mesh, obtained by using different types of elements (tetrahedra, hexahedra or cuboids for 3D problems and triangles or quadrangles for 2D problems). The re-constructors are generally associated with the nodes of the mesh. The use of such elements leads to an easy adaptability of the method to modelling of complex shapes and setting of boundary conditions.

Several commercial codes based on FEM are available and they are widely used for applications linked to computer aided design (CAD) of electromagnetic systems.

* advantages: FEM allows an accurate analysis of real-world systems (complex geometries); it can be easily applied in presence of non-linear magnetic materials. It can be easily formulated in the frequency domain (transient analysis is avoided).
* disadvantages: the computational domain must be bounded, such that approximate boundary conditions are often needed. It has medium to high computational cost and it requires complex post-analysis to derive the complete picture of the results.

2. Finite Difference Method (FDM) [28]

The finite difference method is also based on the solution of Maxwell's Equations in their differential form. This approach starts from the approximation of the spatial derivatives with finite increments, leading to an algebraic system of equations where the unknowns are usually the values of the electromagnetic quantity on the nodes of the mesh. It requires the subdivision of the volume into a regular mesh (usually parallelepipeds), which constitutes a severe restriction to the modelling of complex shapes and to the imposition of boundary conditions. The matrix equations generated by FDM are largely sparse, allowing the use of optimised algorithms for their storage and solution.

* advantages: FDM is a versatile and intuitive modelling technique; it allows effective analysis of real-world systems (complex geometries). It can be easily formulated in the frequency domain (transient analysis is avoided); its computational cost is generally lower than with FEM.
* disadvantages: the computational domain must be bounded, such that approximate boundary conditions are often needed. It is less accurate than FEM as a consequence of spatial re-constructors and type of mesh elements; it requires complex post-analysis to derive the complete picture of the results.

3. Finite Integration technique (FIT) [29]

The Finite Integration Technique (FIT) rewrites the integral form of Maxwell's Equations into a discrete formulation. The resulting algebraic set of equations are suited for numerical simulation, but they also represent the theoretical basis for a discrete electromagnetic field theory. Conservation properties with respect to energy and charge can be proved for this discrete electromagnetic field theory.

* advantages: the use of a consistent dual orthogonal grid in conjunction with an explicit time integration scheme leads to computational and memory-efficient algorithms; conceptually similar to circuital methods, but more accurate and applicable to more complex structures; it is especially suited for transient field analysis in radio frequency applications.
* disadvantages: the computational domain must be bounded, so that approximate boundary conditions are often needed; it requires building a dual mesh in the pre-processing phase.

4. Impedance methods

For low-frequency applications, where the dimensions of the domain are small compared with the wavelength, the impedance method has been found to be efficient as a numerical procedure. It is based on replacing the complex geometric structure with a network of lumped elements accounting for the local electromagnetic properties.

* advantages: it allows set-up of an equivalent circuit model for GA. It is easy to implement and allows one to have a map of the operating conditions of the system.
* disadvantages: with this method, it is difficult to simulate complex geometries and consider the vehicle body. It is less accurate than methods based on the solution of Maxwell's Equations in their differential form (FEM and FDM).

5. Boundary element method (BEM) [30], [31]

The boundary element method is a numerical technique which solves boundary integral equations. It is based on the subdivision of the computational domain into portions with homogenous electromagnetic properties. It largely remains a method used for research and is rarely implemented into commercial or distributed software.
It is often used in hybrid implementations together with FEM, to balance the disadvantages of both methods.

* advantages: limited number of unknowns since they are restricted to boundary domain field values. It provides spatially continuous solutions thanks to the use of the Green function; it does not need bounded domains, so it is useful for far field evaluations.
* disadvantages: some criticalities (approximations of the field values) may occur close to the sources, the boundaries of homogeneous domain portions, in the presence of metallic and ferrite materials. It is suitable for weakly non-homogeneous domains; it has high computational cost, since the matrix is fully populated; available tools are mostly academic, whereas commercial tools are rarely available.

The FEM approach is the most common tool for this type of application. Commercial codes currently make it possible to import the geometries of coils, screens and ferrite concentrators directly from the CAD, and the same applies to the vehicle body. FEM requires skilled and experienced technicians. The critical points are the following:

1. Modelling with adequate discretisation;
2. discretisation of the thicknesses of conductive materials (aluminium and its alloys in particular);
3. assigning the correct physical properties to materials.

The discretisation of the domain must be fine enough to reproduce the quantities of interest (typically the trend of the magnetic field) in a smooth and continuous way, and must ensure the correct reproduction of physical phenomena such as the "skin effect" near the surface of metals. This issue is discussed further in Section 8.1.1 below.

A list of widely used commercially distributed software is reported below. New software is published and commercialised regularly, therefore this list is not exhaustive and other software tools can be found or is expected to be developed after this document has been published.

- Opera 3D (by Simulia): https://www.3ds.com/products-services/simulia/products/opera/
- CST Studio Suite (by Simulia): https://www.3ds.com/products-services/simulia/products/cst-studio-suite/
- Ansys Maxwell: https://www.ansys.com/products/electronics/ansys-maxwell/maxwell-capabilities
- Altair Flux: https://www.altair.com/flux/
- Comsol Multiphysics: https://www.comsol.com/

8.1.1 Suitability of models

Even for the experienced FEM modeler it may not be obvious which geometry discretisation may be the most appropriate and suitable for any given WPT geometry. A conservative approach is to test the computation tool on a simplified geometry, on which the magnetic field distribution is known. As part of the MICEV [24] project, an axisymmetric geometry was used, with the results reported in Appendix D.

Additional issues are related to “what to model” besides coils, ferrite concentrators and aluminium screens, especially what degree of approximation may be introduced into the model with respect to the real-world situation. Two scenarios can be identified:

1. The vehicle has a metallic body, a situation likely to be most common. In this case, the bodywork acts to attenuate the magnetic field and it is necessary to model it to assess the exposure inside the vehicle. Normally, the engine and other metal parts are outside the passenger compartment, leading only to local variations in the magnetic field in the engine compartment, which should not normally be significant for human exposure. In general, conductive and/or ferromagnetic masses like the engine, rims and shafts, has a shielding effect, as the magnetic field is attracted by the metal masses and tends to reduce in the passenger compartment.

2. The vehicle has a predominantly non-metallic body, such as fiberglass. In this case, the metal uprights and all the metal parts (distribution shafts, transmission, engine, rims, etc.) should be modelled, as they could significantly influence the magnetic field distribution inside the passenger compartment that is not shielded by the vehicle metal body. This is the most challenging and potentially most costly situation from a modelling point of view and requires a CAD of the whole vehicle for effective field modelling.

Discretisation and thicknesses of conductive materials

At the frequency of tens of kHz, a consistent skin effect in conductive materials is present. Equation (2) is valid for linear materials like pure conductive materials, or magneto-conductive ideal materials or magneto-conductive materials utilised at constant permeability (causing low variations of the magnetisation at low field values). In this simplified case, the penetration depth, δ, of magnetic fields into the material is given by:

$$\delta = \frac{1}{\sqrt{\pi f \sigma \mu}} \quad (2)$$

where π is a constant with a value of 3.1416..., f is the frequency of the magnetic field in Hz, which is equal to the frequency of the current in the coils, σ is the electrical conductivity in S/m and μ is the permeability of the material.

For example, in an aluminium shield having a conductivity of approximately 30 MS/m, the magnetic field depth of penetration is 0.315 mm at a frequency of 85 kHz. This implies that the discretisation along the shield thickness should have a size of at least one third of the penetration depth, in order to guarantee an adequate modelled reconstruction of the eddy current circulation. Furthermore, given that the thickness of the material is usually 2 mm or 3 mm, a complex non-uniform discretisation will be required, which could lead to a complex mesh that is difficult to manage.

In the presence of conductive materials, it is strongly recommended to use codes that implement the so-called "Impedance Boundary Conditions" (IBC) thus simplifying the management of the 3D mesh in the direction of the material thickness. This also applies to the vehicle-body.

Assignment of the physical properties of the materials to the charging station model

The assignment of the physical properties to the magnetic materials involved in the modelling of a charging station is generally not a simple task as the magnetisation characteristics are measured in static or quasi-static conditions, whereas the working frequency in the charging station ranges between 20 kHz and 85 kHz.

Limited data is available in literature regarding the characteristics of magnetic materials at these working frequencies. Due to the lack of specific data, it is advisable to assign a relative magnetic permeability of 2000 to ferrite, and an electrical conductivity between 30 MS/m and 35 MS/m to aluminium. Regarding the metal sheet of the car-body, some data measured and provided in [32] suggests a relative magnetic permeability of 300 and an electrical conductivity of 2 MS/m for the metal lamination of the vehicle-body.

Glass and fiberglass are transparent to the magnetic field at the working frequencies specified above, and this can lead to particular exposure situations which are discussed in Section 8.1.2.

8.1.2 Critical scenarios

The first step in the identification of critical scenarios giving rise to an increase in the magnetic flux density inside the vehicle compartment is to identify which materials the vehicle body consists of. The next step is to evaluate the size and position of windows, screens, doors open vs closed and cable entries/exits.

A typical example of a vehicle car-body consists of a carbon-steel alloy, which acts as an efficient shield attenuating the magnetic field generated by the WPT system. A plate is located over the WPT system joined to the sides of the vehicle body (including the windows), up to and including the roof.

In the following examples, situations are outlined that may cause an increase in the magnetic field density within the vehicle compartment at the working frequencies.

Vehicle body made of plastics/fiberglass
A fiberglass vehicle-body is transparent to the magnetic field and therefore the bottom/floor must be shielded with an aluminium and/or a ferromagnetic sheet, to protect the passengers. The magnetic field is shielded by two effects: the counter field produced by eddy currents in the conductive material, and the magnetic flux shunting effect due to the magnetic permeability of the ferromagnetic shielding sheet. At the end of the shield, due to its limited area, a border effect is unavoidable and the magnetic field "leaks" into the vehicle, with maximum field strength found near the lateral sides, in the vicinity of the transition between the floor and the wall, where the effect of the shield placed between the coils and the bus floor ceases to be significant. In addition to this, the fiberglass chassis must be reinforced with a metal frame structure. This structure together with the presence of other metallic objects inside the vehicle gives rise to a non-uniform spatial magnetic field inside the vehicle.

Wide glass surfaces
Glass surfaces are completely transparent to the low frequency magnetic field. Therefore, the magnetic field leaks into the vehicle compartment.
In a car with carbon-steel alloy doors, the lowest part of the window begins at a height of approximately 80 cm above the vehicle floor. Due to the glass transparency, higher magnetic field levels inside the compartment are found in the vicinity of the windows. The wider and higher the windows, the larger the magnetic field in the compartment.
In a bus, the entrance is often equipped with sliding doors, which consists to a large extent of glass from floor to roof, where the magnetic field can leak into the compartment.

Open doors vs closed doors
The doors in an urban vehicle are made of carbon-steel alloy and act as a shield. Consequently, the magnetic field at seat level is very low. With doors open, the magnetic field leaks into the vehicle compartment and the magnetic field density at seat level becomes higher.

The effect of the car door (open/closed) is studied in [33] and is shown in Figure 13 for the case of a central WPT. The map of the B-field amplitude is reported at the height z = 0.4 m from the ground. The B-field amplitude outside the vehicle is not significantly affected. However, when the door is open, the B-field leaks into the car. The magnetic induction values drop by three orders of magnitude as one moves inside the car-body, ranging in value from fractions of mT close to GA, to values approaching the ambient noise of < 10 nT inside the car-body. Higher values inside the vehicle (~100 nT) were observed in proximity to glass surfaces, which suffer from a shielding effect.

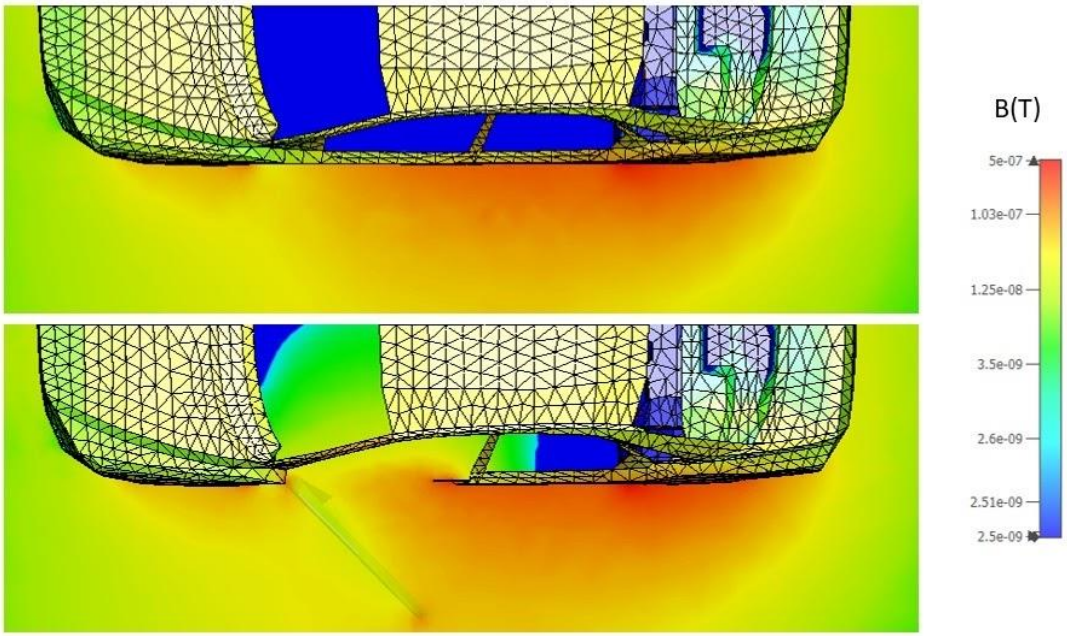

Figure 13. Effect of the door opening on the magnetic field levels (with Rx coil in central position below the car body). The maps of the B-field amplitude are reported at the height z = 0.4 m from the ground: (a) with closed door, (b) with open door [33].

Cable entries

In the vehicle body the cable bundles pass via cable grommets through the floor baseplate or through to the engine compartment. Magnetic fields can leak through these cable grommets resulting in a local magnetic field "hot spot" inside the compartment, especially if the transit point is close to the receiving coil.

8.2 Computation of induced electric field in human bodies

8.2.1 Introduction

Currently, there exists no experimental phantom of the human body that can reliably evaluate and quantify the fields induced in the human body due to WPT systems. Therefore, the quantification of the exposure with respect to basic restrictions must be carried out through numerical modelling backed up by on-site testing. Section 8.1 lists the appropriate numerical methods that can be used to represent the incident magnetic fields of the WPT systems. Most of the numerical methods described above can be also used to calculate the field distribution inside complex anatomical models (induced E-field). This chapter summarises the requirements of the software and the models, suggests how to select relevant exposure scenarios and gives guidance for the numerical evaluation and the assessment of its uncertainty.

8.2.2 Requirements on the numerical methods and on the anatomical models

8.2.2.1 Simulation software

For the simulation of the fields inside a complex anatomical model, the simulation software must fulfil the following requirements:

- numerical representation of the incident magnetic fields over the entire region of the exposed human body through one of the following approaches: (1) simulation of the WPT system and the relevant parts of the vehicle and its environment or (2) import of the measured magnetic fields and reconstruction of the vector potential [34];
- importing, positioning and meshing of appropriate anatomical models (see 8.2.2.2) as well as assignment of the tissue conductivities;
- quantification of the induced fields in terms of the applicable exposure guidelines, such as the average electric field [18, 19].

The requirements on the simulation software as well as the methods for the assessment of correct implementation and evaluation of the induced fields are given in [35].

A list of popular commercially distributed software for computations of induced quantities in anatomical human models, is reported below. New software is published and commercialised regularly, therefore this list is not exhaustive and other software tools can be found or will be developed after this document is published.

- Sim4Life (by ZMT):
  - https://zmt.swiss/sim4life/
- CST Studio Suite (by Simulia):
  - https://www.3ds.com/it/prodotti-e-servizi/simulia/prodotti/cst-studio-suiter/
- Altair Feko:
  - https://www.altair.com/feko/

8.2.2.2 Anatomical models

The anatomical models that are used for the quantification should consider the exposed population as described in 8.2.3. The main parameters for the quantification are the body mass and height of the models. These parameters define the exposed cross section of the anatomical model, which is one of the most relevant quantities to determine the exposure. However, the complex distribution of the dielectric properties inside the body (tissues with low and high electric conductivity, such as the skin, fat, the brain or muscles) or particular body postures also contribute to the variability of the exposure and must be appropriately considered by the anatomical model. A large number of accurate anatomical models covering the age range of the entire human lifespan is available from [36]. An appropriate database for tissue conductivities can be found in [37].

8.2.3 Selection of exposure scenarios

For the conservative quantification of the exposure, the modelling of a large number of exposure scenarios may be required. Exposure scenarios should consider a) intended and b) unintended exposure. Intended exposure to WPT systems includes the exposure of passengers or bystanders as described in 7.1.6 and considers normal operation conditions, for example, with respect to the distances of the exposed persons from the coils of the WPT system. Unintended use may occur, for example, if normal operational distances cannot be

maintained, if particular body postures lead to an increased exposure, or if exposed people do not belong to the target population, such as infants (in strollers), pregnant women, sick or disabled (wheelchair users), wearers of metallic implants, etc. It should also be noted that smaller bodies (children) may be able to come closer to the WPT system compared to larger adult bodies. In summary, the choice of the exposure scenarios to be simulated should consider:

- minimum possible exposure distance that a person can reach in the space under the vehicle or between the coils, or people walking or crouching close to the WPT station;
- maximum possible coupling, that is large body cross section;
- postures that may increase the exposure, such as loops formed by limbs or by people touching each other or by touching the metal parts of a stroller or a wheelchair.

In summary, the exposure scenarios should be defined in terms of:

- physiological parameter range of the exposed population such as body mass and height, age, etc.;
- distance from the WPT system or the vehicle;
- posture with respect to the WPT system (standing, lying, etc.) as this affects the exposed cross section of the body;
- particular body postures that have been considered or excluded.

Appropriate rationales for the choice of the exposure scenarios should be given.

Based on the numerical results and comparison against basic restrictions ([17-18], see Section 6), the exposure scenarios that violate the safety limits should be identified. The procedure, facility and precautions to prevent such exposure conditions should be explained and implemented by the specific WPT system.

8.2.4 Numerical evaluation

For the numerical simulation of the exposure scenarios, the computational domain should be chosen to be large enough to accommodate the entire body of the exposed person. Depending on the characteristics of the WPT system, modelling of the entire vehicle may not be required. See Sections 7.1.6 and 8.1.1 for the relevant characteristics of the vehicle.

Before the exposure is quantified in the anatomical models, the incident field must be modelled with sufficient accuracy (see Sect. 8.1.1). As mentioned in 8.1, this can be done by importing measured field data or by modelling the WPT system and, if required, the relevant parts of the vehicle. Recommendations for the modelling of the WPT system and the vehicle are given in [35]. The model should be validated by comparison of the simulated field strength and distribution with measurement data. An appropriate validation approach considering the uncertainties of both the numerical and the experimental methods is given in [35]. Guidance on the quantification of the numerical uncertainty is also given in 8.2.5.

Before the quantification of the exposure scenarios, the impact of the solver settings should be assessed, and the simulation setup should be reviewed for technical correctness. This can be done by simulation of one representative case among the exposure scenarios. The assessment of the solver settings includes:

- mesh resolution: the mesh resolution of the anatomical model should be sufficiently fine to avoid meshing-dependent effects on the simulation result. The required resolution should be determined by repeated simulation of the same exposure scenario until convergence is reached. Typically, the mesh resolution should not

exceed 2 mm for the correct representation of the anatomical details of the body model. An initial simulation can be run to identify hot spots in the body. The spatial resolution in the areas of these 'hot spots' (high field locations) may require particular attention. In fact, numerical solutions computed on voxel-based models are usually affected by numerical artefacts, as discussed by several authors [38], [39], [36]. The main causes of numerical artefacts are the stair-casing error [41], inevitable when using voxelised models, and the contrast between electromagnetic properties of adjacent voxels belonging to different tissues. In addition, local artefacts may occur due to voxelisation that are not present in the original CAD of the human body; these artefacts appear especially in proximity of the skin (with reference to skin-to-skin contact voxels, see [20]);

- tissue integrity: the meshing of thin tissue layers, regions with high dielectric contrast or tissues forming loops may require particular attention, for the same reasons mentioned above;
- tissue conductivity: the impact of the uncertainty in the tissue conductivities on the dosimetric result should be quantified. [42] reports a spread of the measured data for the dielectric tissue models of up to 25 % for frequencies below 100 kHz. The tissue parameters in the simulation should be varied within this order of magnitude. If we account for 25 % variation in tissue conductivity, the corresponding maximum change in the electric field and current density will be <55 %. The SAR will change maximally by <74 %. In case these uncertainties are detrimental for a specific system design and a more accurate, i.e. less conservative, uncertainty value is needed, a comprehensive sensitivity analysis needs to be performed including all tissues in the exposed volume (Appendix E);
- model truncation: as mentioned above, the entire anatomical model should be included in the computational domain. If this is not possible, for example due to memory limitations, regions of low exposure may be truncated if and only if it is demonstrated that the impact of this truncation has negligible impact on the final result;
- solver convergence: the impact of the convergence of the numerical solver on the exposure evaluation should be quantified;
- sanity check: the simulation results should be compared to previous simulations, to standardised benchmark cases for which a solution is available or to analytical solutions of a similar exposure scenario.

The exposure should be evaluated according to the basic restrictions as defined in Section 6 and Appendix B. Guidance on the numerical implementation of the evaluation is given in [34]. The results should be reported in terms of a representative case that can be assumed to be conservative for the majority of exposure scenarios. In addition, the worst-case exposure (including the configuration for which it was observed) and the variability of the exposure considering all evaluated cases should be indicated. The results should be reported together with their combined numerical and experimental uncertainty (8.2.5).

8.2.5 Considerations for the uncertainty evaluation

In addition to the experimental uncertainty (Section 7.2.2), the numerical uncertainty should be assessed. The quantification of the numerical uncertainty requires the assessment of the change of exposure results in terms of:

- mesh resolution;
- dielectric parameters of the tissues;
- dimensions of the computational domain and truncation of the model;
- solver convergence;
- positioning accuracy with respect to the WPT system and the vehicle;
- sensitivity to physical properties of magnetic and conductive materials;
- positioning accuracy with respect to the WPT system and the vehicle;

- boundary conditions if applicable, e.g., for grounding;
- import of the measured fields and interpolation.

Details of most of these parameters are discussed in 8.2.4. A detailed discussion of the evaluation of the numerical uncertainty and its parameters can be found in [35].

The compliance of inductive power systems with international recommendations regarding the *in-situ* level of exposure needs accurate predictions and assessment of the radiated magnetic field on a possible bystander position. This task requires not only a fine description of the inductive power system and its environment, but also an adequate 3D modelling software. However, in realistic configurations, the computational cost is heavy: each new set of parameters, including geometrical characteristics, material properties, possible misalignment and distance between transmitter and receiver, leads to a new 3D complex problem to solve. The stochastic models based on Kriging and Polynomial chaos expansions provided a fast approach to estimate uncertainty contributions and variabilities of different parameters, both physical and geometrical. Specifically, where there is a reduced number of 3D full wave computations (samples), the combination of Kriging and Polynomial chaos expansion provides a very good predictor [32]. The analysis of a realistic and complex situation, including a light vehicle, showed that for a given set of parameters, relying on 50 % of the total number of sample data points is accurate enough to build a correct sensitivity analysis relevant to the level of exposure [43]. Also, the influence of the relative permeability and the coil misalignment along the axis of motion is clearly negligible against the misalignment along the other axes and the car-body conductivity.

Numerical aspects related to the accuracy and the computational efficiency of numerical dosimetric simulations are widely discussed in [40], where two alternative numerical methods for dosimetric analysis, respectively based on electric vector potential and electric scalar potential formulations, are compared for the electric field computation in highly detailed anatomical human models. The analysis has highlighted a different behaviour of the two alternative finite element formulations, depending on the characteristics of the voxelised anatomical human model and spatial distribution of the magnetic field. It is difficult to draw general conclusions in terms of the most robust method for dosimetric solutions. Nevertheless, the results obtained with the two formulations after applying the filtering techniques tend to converge. Furthermore, the use of the filtering technique adopted in the study has demonstrated its capability to assess the results, removing undesirable outliers and reducing discrepancies between results obtained with different solvers to less than 10 % for 1 mm anatomical model resolutions.

8.2.6 Example of dosimetric analysis

An example of a dosimetric analysis considering both realistic WPT systems of light and heavy vehicles is summarised here. The entire set of results can be found in [33].

8.2.6.1 Exposure of a light vehicle

A realistic model of a Volvo S80 sedan, supplied by Volvo Car Company, was used in this analysis. Two receiving coil positions were considered: (1) at the front of the car and (2) at the centre of the car (see Figure 14). The WPT system has a rated power of 7.7 kW and a switching frequency close to 85 kHz. The exposure was assessed for the human anatomical models placed in the positions shown in Figure 14.c and 14.d. The most relevant analysed exposure scenarios are summarised in Table 6, referencing the advanced high resolution anatomical Virtual Population (ViP) models *Charlie*, *Thelonious* and *Duke* [35].

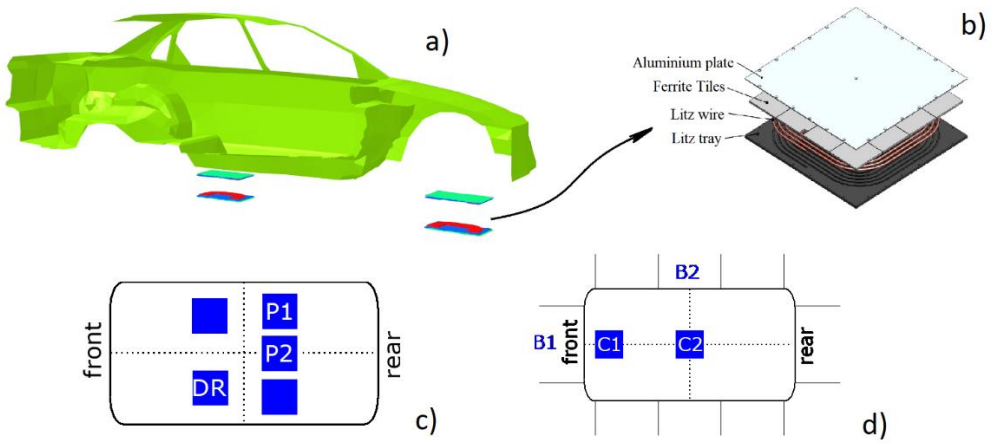

Figure 14. S80 Volvo car-body cross section and location of the coil charging system (a), together with the coil pad constructed according to SAE J2954 standard (b). Positions of the driver (DR) and two passengers (P1 and P2) sitting inside the car (c), and general position of the coil under the car (C1 and C2) and of two by-standers (B1 and B2) (d).

Table 7. The analysed exposure scenarios. The table refers to the positions of the WPT systems and the possible locations outside and inside the car as shown in Figure 14.

WPT System Position	ViP Model Position	Posture
Central/Front	B2/B1	*Duke* standing
Central/Front	B2/B1	*Duke* crouching on knees
Front	B1	*Duke* lying with arm stretched
Central/Front	B2/B1	*Thelonious* sitting
Central	inside the car	*Charlie* (P2), *Duke* (DR) and *Thelonious* (P3) sitting

Figure 15 shows the results for the given exposure scenarios, compared against the basic restriction level given in ICNIRP 2010 (Section 5). The standing posture represents the safest exposure condition, whereas the induced E-field approaches the basic restriction (BR) when the ViP phantoms move closer to the source.

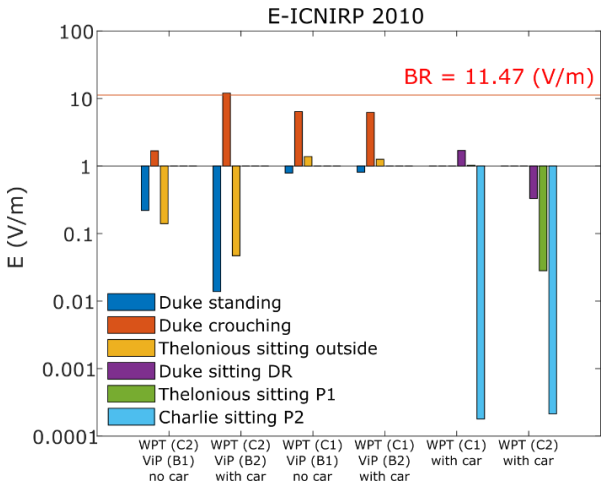

Figure 15. Peak of the E-field (V/m) averaged according to ICNIRP 2010 guidelines induced in the ViP phantoms. The horizontal red line represents the basic restriction (BR) level for induced E-field at 85 kHz according to ICNIRP 2010.

8.2.6.2 Exposure of a bus

The schematic for exposure assessment in proximity to and inside a bus with a rated power of 50 kW and a switching frequency close to 27.8 kHz, is shown in Figure 16. More information on the bus charging station can be found in Appendix A. Table 8 summarises the most relevant exposure scenarios and the corresponding results are given in Table 9 for carbon-steel alloy and fiberglass bus-bodies. Results are compared against BR levels for induced E-field at 27.8 kHz according to ICNIRP 2010 (BR = 3.75 V/m) [17]. The induced values were lower in all cases other than the light car, except when the *Duke* model is in crouching posture outside the bus. In terms of induced E-field, the fiberglass bus-body increases the induced exposure up to 35 % with respect to the metal car-body.

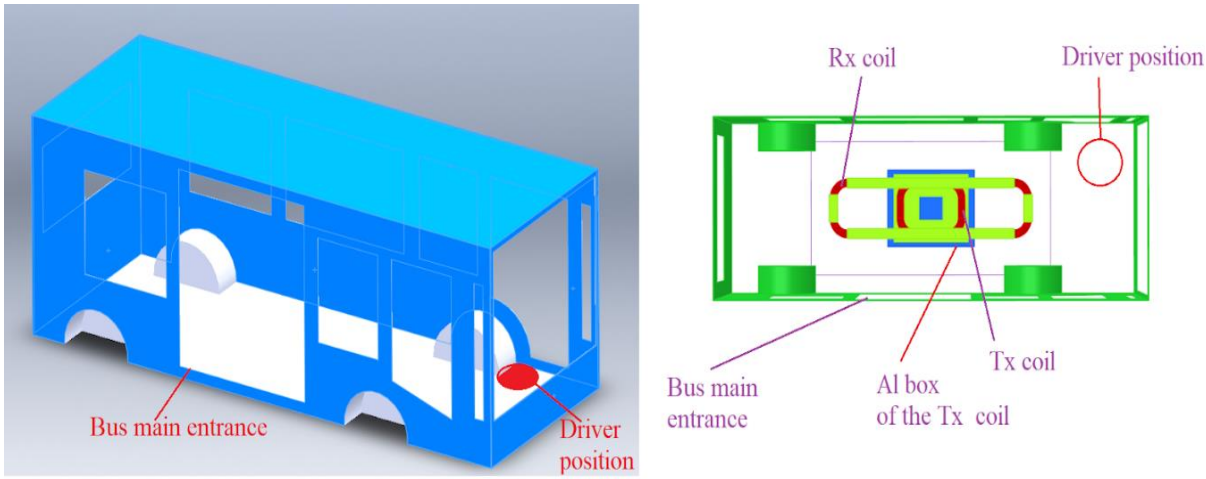

Figure 16. Bus body: a) 3D representation, b) plan view. The Tx coil size is 0.8 m x 0.6 m and the on-board Rx coil is 2.5 m x 0.6 m. The total length of the bus is 5.1 m, while the total width is 2.3 m.

Table 8. The exposure scenarios were analysed to assess exposure to the WPT system for charging the electric bus. The WPT system was located under the bus in the central position.

WPT System Position	ViP Model Position	Posture
Central	outside/front of the door	*Duke* standing
Central	outside/front of the door	*Charlie* sitting
Central	outside/front of the door	*Duke* crouching
Central	outside/front of the door	*Thelonious* sitting
Central	inside/front of the door	*Duke* sitting
Central	inside/front of the door	*Charlie* sitting

Table 9. E-fields induced in ViP phantoms due to the magnetic field generated by the WPT system for charging the electric bus for the exposure scenarios described in Table 8.

ViP Model Position	Posture	E-ICNIRP (V/m) (in bracket the ratio with respect to the limit)
	Carbon-steel alloy bus-body	
outside/central	*Duke* standing	0.3 (0.08)
outside/central	*Charlie* sitting	0.2 (0.05)
outside/central	*Duke* crouching	4.2 (1.12))
outside/central	*Thelonious* sitting	0.6 (0.16)
Inside	*Duke* standing	0.2 (0.05)
Inside	*Charlie* sitting	0.2 (0.05)
	Fiberglass bus-body	
outside/ central	*Duke* standing	0.4 (0.01)
outside/ central	*Charlie* sitting	0.2 (0.06)

8.2.7 Considerations on implanted medical devices

The presence of a conductive medical implant with electrical conductivity much greater than that of the surrounding tissues leads to large localised field enhancements in the human body. Such a field enhancement potentially results in exceeding the basic restrictions even for exposure values that are below the reference limits [44]. The importance of this issue has been recognised in the domain of magnetic resonance imaging (MRI) exposure safety, where the results of extensive research show that the presence of elongated implants in patients undergoing MRI scans poses a potential health risk. To support development and certification of implants that are MRI safe, assessment standards (e.g. ISO-TS 10974:2012 (2012)) have been established. A similar framework is also required for WPT stations, which constitutes the focus of this section.

WPT stations operate at frequencies below 1 MHz, where the wavelength is drastically larger than the typical implant lengths. This is in contrast with typical MRI systems operating at 10-100 MHz frequency range, where active implants are usually electrically long enough (i.e. more than 20 % of the relevant wavelength in tissue) for resonance effects to occur. In the low-frequency operation range of WPT stations, tip enhancement effects and tissue conductivity contrast are the main origins of the field enhancement. Therefore, distinct models and assessment approaches need to be developed concerning the safety of WPT fields for human bodies carrying implanted devices. In [44], a mechanistic model is developed for the safety assessment of short implants. Based on the proposed approach, the following procedure should be followed to ensure the safety of WPT station for generic and worst-case implants:

1) a single reference simulation, or experimental measurement, per tip-shape of homogeneous exposure within a semi-homogeneous tissue is performed to characterise the tip-related resistance and field distribution. This study delivers the functions $f(s)$ and $g(s)$ in equations (1) to (4) of [44];
2) *in vivo* incident field conditions are determined (these could be precomputed for the relevant exposure scenarios and reused for different devices);

3) the local exposure metrics are predicted, based on the mechanistic model, by combining the reference simulation with the *in vivo* incident field conditions and information about the tissues surrounding critical exposed implant locations.

The predicted data in step 3) contains all the relevant quantities of interest for the safety assessment, such as peak electric field. These data will then be considered to certify the safety of the WPT station.

9. Conclusions

With this guide, the reader can orient himself/herself among the numerous standards that either exist already or will be published, which are related to the topic of inductive charging of electric vehicles. The reader will gain clear tools and limits for a correct assessment of the EMF exposure from vehicle Wireless Power Transfer systems. Finally, the reader will be able to more easily apply the internationally recognised standards to their work, by gaining extra knowledge and additional tools to carry out the complex experimental and computational task of EMF exposure assessment.

10. Acknowledgements

This work is part of the European project “16ENG08 MICEV — Metrology for inductive charging of electric vehicles”. This project has received funding from the European Metrology Programme for Innovation and Research (EMPIR) programme co-financed by the Participating States and from the European Union’s Horizon 2020 research and innovation programme.

11. References

[1] SAE TIR standard J2954, “WPT for Light Duty Plug In/ EVs and Alignment Methodology”, May 2016, last revision 2019/04/23.

[2] IEC 61980-1:2020, Edition 2.0 (2020-11-19), “Electric vehicle wireless power transfer (WPT) systems - Part 1: General requirements,” International Electrotechnical Commission (IEC), IEC, Geneva, Switzerland, 2020.

[3] IEC TS 61980-2:2019, Edition 1.0 (2019-06-13), “Electric vehicle wireless power transfer (WPT) systems - Part 2: Specific requirements for communication between electric road vehicle (EV) and infrastructure,” International Electrotechnical Commission, IEC, Geneva, Switzerland, 2019.

[4] EC TS 61980-3:2019, Edition 1.0 (2019-06-13), “Electric vehicle wireless power transfer (WPT) systems - Part 3: Specific requirements for the magnetic field wireless power transfer systems,” International Electrotechnical Commission, IEC, Geneva, Switzerland, 2019.

[5] IEC TS 61000-3-4:1998 “Electromagnetic compatibility (EMC) - Part 3-4: Limits - Limitation of emission of harmonic currents in low-voltage power supply systems for equipment with rated current greater than 16 A,” International Electrotechnical Commission, IEC, Geneva, Switzerland, 1998.

[6] IEC TS 61000-3-5:2009 “Electromagnetic compatibility (EMC) - Part 3-5: Limits - Limitation of voltage fluctuations and flicker in low-voltage power supply systems for equipment with rated current greater than 75 A,” International Electrotechnical Commission, IEC, Geneva, Switzerland, 2009.

[7] IEC 61000-6-3:2020, “Electromagnetic compatibility (EMC) - Part 6-3: Generic standards - Emission standard for equipment in residential environments,” International Electrotechnical Commission, IEC, Geneva, Switzerland, 2020.

[8] CISPR 11:2015+AMD1:2016+AMD2:2019 CSV Consolidated version, “Industrial, scientific and medical equipment - Radio-frequency disturbance characteristics - Limits and methods of measurement,” International Electrotechnical Commission, IEC, Geneva, Switzerland, 2019.

[9] CISPR 12:2007, “Vehicles, boats and internal combustion engines - Radio disturbance characteristics - Limits and methods of measurement for the protection of off-board receivers,” International Electrotechnical Commission, IEC, Geneva, Switzerland, 2007.

[10] CISPR 25:2016, “Vehicles, boats and internal combustion engines - Radio disturbance characteristics - Limits and methods of measurement for the protection of on-board receivers,” International Electrotechnical Commission, IEC, Geneva, Switzerland, 2016.

[11] ISO 16750-2:2012, “Road vehicles — Environmental conditions and testing for electrical and electronic equipment — Part 2: Electrical loads,” International Organization for Standardization, ISO, Geneva, Switzerland, 2012.

[12] ISO 26262, “Road vehicles — Functional safety,” International Organization for Standardization, ISO, Geneva, Switzerland.

[13] ISO 6469-1:2019, “Electrically propelled road vehicles — Safety specifications — Part 1: Rechargeable energy storage system (RESS),” International Organization for Standardization, ISO, Geneva, Switzerland, 2019.

[14] ISO 6469-2:2018, “Electrically propelled road vehicles — Safety specifications — Part 2: Vehicle operational safety,” International Organization for Standardization, ISO, Geneva, Switzerland, 2018.

[15] ISO 6469-3:2018, “Electrically propelled road vehicles — Safety specifications — Part 3: Electrical safety”, International Organization for Standardization, ISO, Geneva, Switzerland, 2018.

[16] ISO 19363:2020, “Electrically propelled road vehicles — Magnetic field wireless power transfer — Safety and interoperability requirements,” ISO, Geneva, Switzerland, 2020.

[17] ICNIRP, “Guidelines for limiting exposure to time-varying Electric and magnetic fields (1Hz – 100 kHz),” Health Physics 99(6):818-836; 2010.

[18] ICNIRP, “Guidelines for limiting exposure to time-varying electric, magnetic and electromagnetic fields (up to 300 GHz)”, Health Physics, vol. 74, pp. 494–522, 1998.
[19] ICNIRP. “Guidelines for limiting exposure to time-varying electric, magnetic and electromagnetic fields (up to 300 GHz)”, Health Physics, vol. 118, 483-542, 2020.
[20] IEEE Std C95.1™-2019 (Revision of IEEE Std C95.1-2005/ Incorporates IEEE Std C95.1-2019/Cor 1-2019), “IEEE Standard for Safety Levels with Respect to Human Exposure to Electric, Magnetic, and Electromagnetic Fields, 0 Hz to 300 GHz”, IEEE, New York, USA, 2019.
[21] RIVM, “Comparison of international policies on electromagnetic fields (power frequency and radiofrequency fields),” National Institute for Public Health and the Environment, RIVM, Bilthoven, The Netherlands, 2018. https://www.rivm.nl/sites/default/files/2018-11/Comparison%20of%20international%20policies%20on%20electromagnetic%20fields%202018.pdf.
[22] ISO 14117:2019(E), “Active implantable medical devices — Electromagnetic compatibility — EMC test protocols for implantable cardiac pacemakers, implantable cardioverter defibrillators and cardiac resynchronization devices,” ISO, Geneva, Switzerland, 2020.
[23] O. Bottauscio, M. Chiampi, G. Crotti and M. Zucca “Probe influence on the measurement accuracy of nonuniform LF magnetic fields,” IEEE transactions on instrumentation and measurement 54 (2), 722-726, 2005.
[24] M. Zucca et al., “Metrology for Inductive Charging of Electric Vehicles (MICEV),” Proc. International Conf. of Electrical and Electronic Technologies for Automotive 2019 (AEIT Automotive), 2019, pp 1-4.
[25] F. Li, D. Hart, I. Fatadin, R. Ferguson, R. Guilizzoni and S. Harmon, “Characterisation of an Optical 2D Tracking System,” 2019 IEEE 2nd British and Irish Conference on Optics and Photonics (BICOP), London, United Kingdom, 2019, pp. 1-4, doi: 10.1109/BICOP48819.2019.9059570.
[26] JCGM, J. JCGM 100-2008: Evaluation of Measurement Data – Guide to the Expression of Uncertainty in Measurements. Jt. Comm. Guid. Metrol. 2008.
[27] E.B. Becker, G.F. Carey, J.T. Oden, Finite Elements (four volumes), Prentice-Hall, Englewood Cliffs, 1981.
[28] M.V.K. Chari, S.J. Salon, Numerical Methods in Electromagnetism, Academic Press, New York, 2000.
[29] P. Alotto, F. Freschi, M. Repetto, C. Rosso, The Cell Method for Electrical Engineering and Multiphysics Problems: An Introduction, Lecture Notes in Electrical Engineering, Springer, 2013.
[30] W.S. Hall, The Boundary Element Method, Kluwer Academic Publisher, London, 1994.
[31] P.K. Banerjee, R. Butterfield, Developments in Boundary Element Methods (two volumes), Applied Science Publishers, London, 1979.
[32] L. Pichon, P. Lagouanelle and S. Deshmukh, “Assessment of Human Exposure in Case of Wireless Power Transfer for Automotive Applications using Stochastic Models,” Applied Computational Electromagnetics Society Journal 35, 6 pages, 2020.
[33] I. Liorni, O. Bottauscio, R. Guilizzoni, P. Ankarson, J. Bruna, A. Fallahi, S. Harmon and M. Zucca, “Assessment of Exposure to Electric Vehicle Inductive Power Transfer Systems: Experimental Measurements and Numerical Dosimetry,” Sustainability 12 (11), 4573 (25 pages), 2020.
[34] I. Laakso, V. De Santis, S. Cruciani, T. Campi and M. Feliziani, “Modelling of induced electric fields based on incompletely known magnetic fields,” Physics in Medicine & Biology, vol. 62, no. 16, pp. 6567, 2017.
[35] IEC/IEEE PAS 63184 “Assessment methods of the human exposure to electric and magnetic fields from wireless power transfer systems – Models, instrumentation and numerical methods and procedures (Frequency range for 1 kHz to 30 MHz), 2021.
[36] M. C. Gosselin et al., “Development of a new generation of high-resolution anatomical models for medical device evaluation: the Virtual Population 3.0. Physics in Medicine & Biology,” 59(18), 5287, 2014.

[37] P. A. Hasgall et al., “IT’IS Database for thermal and electromagnetic parameters of biological tissues,” Version 4.0, May 15, 2018, DOI: 10.13099/VIP21000-04-0. itis.swiss/database.
[38] J. Gomez-Tames, I. Laakso, Y. Haba, A. Hirata, D. Poljak and K. Yamazaki, “Computational artifacts of the in-situ electric field in anatomical models exposed to low-frequency magnetic field,” IEEE Trans. Electromagn. Compat., vol. 60, no. 3, pp. 589–597, Jun. 2018.
[39] A. Hirata et al., “Intercomparison of induced fields in Japanese male model for ELF magnetic field exposures: Effect of different computational methods and codes,” Radiat. Prot. Dosimetry, vol. 138, pp. 237–244, 2010.
[40] A. Arduino, O. Bottauscio, M. Chiampi, L. Giaccone, I. Liorni, N. Kuster, L. Zilberti, M. Zucca, “Accuracy Assessment of Numerical Dosimetry for the Evaluation of Human Exposure to Electric Vehicle Inductive Charging Systems”, IEEE Transactions on Electromagnetic Compatibility, Vol. 62, No. 5, 2020, pp. 1939-1950.
[41] D. Poljak et al., “On the use of conformal models and methods in dosimetry for nonuniform field exposure,” IEEE Trans. Electromagn. Compat., vol. 60, no. 2, pp. 328–337, Apr. 2018.
[42] S. Gabriel, R. W. Lau and C. Gabriel, “The dielectric properties of biological tissues: Ii. measurements in the frequency range 10 Hz to 20 GHz”, Physics in medicine & biology, vol. 41, no. 11, pp. 2251, 1996.
[43] P. Lagouanelle, O. Bottauscio, L. Pichon and M. Zucca, “Impact of parameters variability on the level of human exposure due to inductive power transfer,” 19th Biennial IEEE Conference on Electromagnetic Field Computation (CEFC), Pisa, Italy, November 16-19, 2020.
[44] I. Liorni, E. Neufeld, S. Kühn, M. Murbach, E. Zastrow, W. Kainz and N. Kuster, “Novel mechanistic model and computational approximation for electromagnetic safety evaluations of electrically short implants,” *Physics in Medicine & Biology*, *63*(22), 225015, 2018.
[45] A. Ahmad, M. S. Alam and R. Chabaan, “A Comprehensive Review of Wireless Charging Technologies for Electric Vehicles,” IEEE Transactions on Transportation Electrification, vol. 4, no. 1, pp. 38-63, March 2018, doi: 10.1109/TTE.2017.2771619.
[46] VICTORIA Project, [online] Available: http://greentechlatvia.eu/wp-content/uploads/bsk-pdf-manager/1-8_Project_Victoria_(Bludszuweit)_8.pdf.
[47] C. Andreas, W. Kainz, G. H. Eckhart, K. Honegger, M. Zefferer, E. Neufeld, W. Rascher et al., "The Virtual Family—development of surface-based anatomical models of two adults and two children for dosimetric simulations," *Physics in Medicine &* Biology, 55(2), N23, 2009.
[48] M. C. Gosselin, E. Neufeld, H. Moser, E. Huber, S. Farcito, L. Gerber, M. J. et al., "Development of a new generation of high-resolution anatomical models for medical device evaluation: the Virtual Population 3.0.," *Physics in Medicine & Biology 59(18)*, 5287, 2014.
[49] P. A. Hasgall, F. Di Gennaro, C. Baumgartner, E. Neufeld, M. C. Gosselin, D. Payne, A. Klingenböck, and N. Kuster, "IT’IS Database for thermal and electromagnetic parameters of biological tissues," Version 3.0, 2015.
[50] P. A. Hasgall, F. Di Gennaro, C. Baumgartner, E. Neufeld, B. Lloyd, M. C. Gosselin, D. Payne, A. Klingenböck, and N. Kuster, "IT’IS Database for thermal and electromagnetic parameters of biological tissues, Version 4.0.," IT’IS, 2018.

Appendix A – A WPT charging station for heavy vehicle

The WPT charging station was developed by CIRCE as part of the Victoria project [45]-[46] and was updated for the MICEV project at the CIRCE facilities, as required by activity A4.2.7.

CIRCE developed the entire system for research into both the power electronics and the inductive power transmission at 50 kW. The wireless power transmission has different modes depending on the duration of the charge required in each case:

1) a stationary and a static in-route transfer system that charges in tens of minutes;

2) a dynamic charger which performs charging in around 2 seconds, while the electric vehicle is passing above the emitting coil, without stopping.

The WPT system transfers energy through inductive coupling between coils separated by a defined distance. The transferred power depends on the geometry of the system, the spatial distribution, shape, size and cross-section of the coils and the operating frequency. At the operating frequency, the transmitter (Tx) and receiver (Rx) coil circuits resonate and, therefore, high power transfer is achieved at great efficiency, reaching an optimal working point.

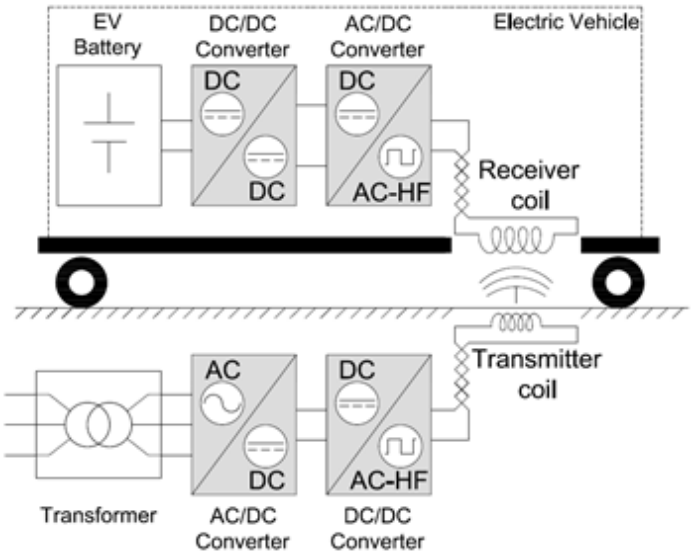

Figure A1. General CIRCE WPT block diagram.

Advantages of the CIRCE development:

- Rx is longer than Tx, leading to improved shielding and longer charging power pulses;
- high efficiency under misaligned conditions;
- safe system design, which tolerates large misalignments even assuming control failure;
- very-low total harmonic distortion (THD) in the grid side <2 %, even in the supra-harmonic frequency range up to 150 kHz;
- operates above audio frequencies in the medium-frequency range at approximately 25 kHz;
- full control of power factor (i.e. ratio between real power and apparent power);
- low power losses, leading to higher efficiency;

- series parallel – series (SP-S) topology in the resonant filter (CIRCE patent), which lets the system operate despite misalignments along the X and Y axes and within distance variation between Tx and Rx, due to different vehicle loads;
- the power electronics system detects the bus position, in order to transfer the energy just at the precise moment;
- the electric vehicle used is a Gulliver U5 20 ESP/LR, 100 % electric bus, with self-guided control to ensure the correct speed and misalignment. The bus was adapted for conductive and WPT fast charging;
- one stationary inductive charge and eight dynamic chargers are connected to the 'DC-bus' and distributed along 100 meters. There are also identical coupling coils both for static and dynamic charging.

The power electronics configuration 'floor' consists of an AC/DC grid multilevel converter, with its 'DC-bus', and a DC/AC medium-frequency bridge converter, which supplies the primary WPT resonant tank with a square wave, with series-parallel topology. The energy transfers wirelessly to the secondary WPT 'resonant tank' embedded into the vehicle, with series topology, and an AC-MF/DC secondary converter, the system supplies power to the electric vehicle batteries.

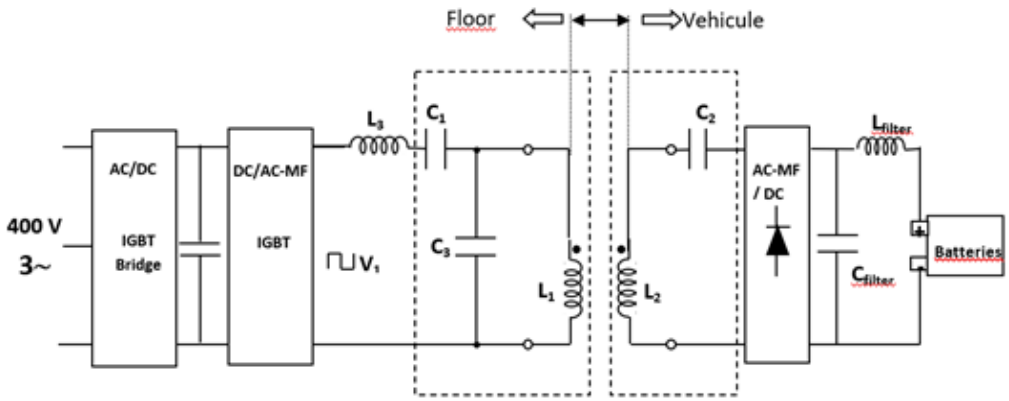

Figure A2. Block diagram WPT configuration.

The main specifications of the power electronics system are:

- rated power: 50,000 W;
- WPT switching frequency: 27,500 Hz. It can be adjusted from 25,000 Hz to 28,000 Hz;
- converters topology: IGBT based;
- type of inductive EV charge: stationary, static, or dynamic charge;
- type of conductive EV charge: CHAdeMO standard;
- output voltage range between 50 and 500 Vdc, and current from 0 to 125 A;
- hardware and software protections: overvoltage, overcurrent, over temperature, malfunction, IGBT failure, magnetothermal and differential current breakers, ground shielding, magnetic field shielding, mechanical protections, among others;
- the AC/DC grid multilevel converter is neutral point clamped (NPC) based, with three-level IGBT converters and no audible noise due to the 20 kHz switching. As a result, there is a very low total harmonic distortion, a reduction in the cost and size, and increased efficiency;
- the electric vehicle bus contains a pack of Li-ion batteries connected in series, with a total energy of 27,2 kWh, a capacity of 75 Ah, and a rated voltage of 362 Vdc. It has a battery management system (BMS) which communicates through Controller Area Network (CAN) bus.

The WPT was designed after extensively considering: EMI shielding, electrical insulation, thermal management, selecting suitable ferrites and Litz wire, connections, materials choice, assembly, and final location.

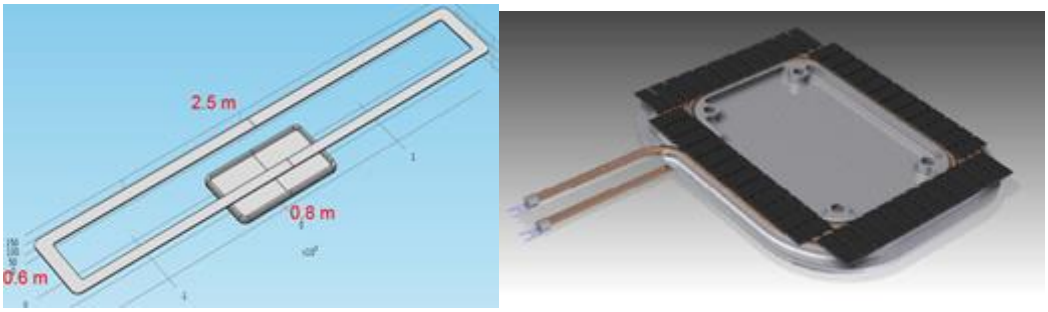

Figure A3. Transmitter L1 and receiver L2 (longer one) WPT coils (isometric view), and L1 3D CAD design.

To comply with ICNIRP 2010 Basic Restrictions [17], the reference level for occupational exposure to time-varying electric and magnetic fields, for a 25 kHz frequency system must be below 100 μT. After simulating the magnetic field distribution between the WPT emitting and receiving coils and the outside enclosure field, the theoretical maximum magnetic field was 27 μT, complying with the regulations.

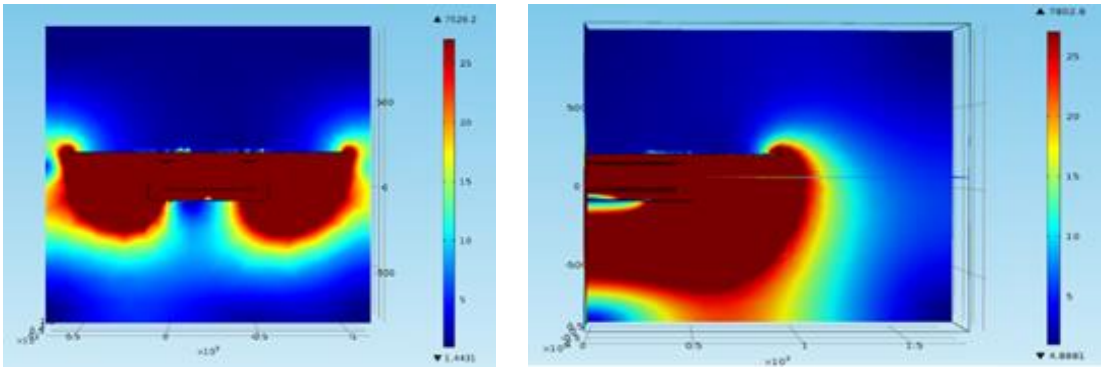

Figure A4. Magnetic field distribution simulation of the emitting and receiving WPT coils. Front and side views.

The WPT charging station is able to transfer 50 kW in stationary (static) charge reaching up to 92 % efficiency when the emitting and receiving coils (primary and secondary, L1 and L2) are aligned, and up to 80 % with misalignments.

Appendix B – ICNIRP 2010 limits (Informative)

Table B1. ICNIRP 2010 basic restrictions for human exposure to time-varying electric and magnetic fields [17].

Exposure characteristic	***Frequency range***	***Internal electric field (V/m) rms***
Occupational exposure		
CNS tissue of the head		
	1-10 Hz	0.5/f
	10 Hz – 25 Hz	0.05
	25 Hz−400 Hz	2×10^{-3}f
	400 Hz−3 kHz	0.8
	3 kHz−10 MHz	2×10^{-4}f
All tissues of head and body	1 Hz−3 kHz	0.8
	3 kHz−10 MHz	2×10^{-4}f
General public exposure		
CNS tissue of the head	1-10 Hz	0.1/f
	10 Hz – 25 Hz	0.01
	25 Hz−1000 Hz	4×10^{-4}f
	1000 Hz−3 kHz	0.4
	3 kHz−10 MHz	1.35×10^{-4}f
All tissues of head and body		
	1 Hz – 3 kHz	0.4
	3 kHz−10 MHz	1.35×10^{-4}f

Notes:

- f is the frequency in Hz.
- In the frequency range above 100 kHz, RF specific basic restriction need to be considered separately.

Table B2. ICNIRP 2010 reference levels for time-varying contact currents from conductive objects [17].

Exposure characteristic	***Frequency range***	***Maximum contact current (mA)***
Occupational exposure	Up to 2.5 kHz	1
	2.5 kHz − 100 kHz	0.4f
	100 kHz − 10 MHz	40
General public exposure	Up to 2.5 kHz	0.5
	2.5 kHz − 100 kHz	0.2f
	100 kHz − 10 MHz	20

Notes: f in kHz.

Table B3. ICNIRP 2010 reference levels for general public exposure to time varying electric and magnetic fields (unperturbed rms values) [17].

Frequency range	***E-field strength E (kV/m)***	***Magnetic field strength H (A/m)***	***Magnetic flux density B (T)***
1 Hz−8 Hz	5	$3.2 \times 10^4/f^2$	$4 \times 10^{-2}/f^2$
8 Hz−25 Hz	5	$4 \times 10^3/f$	$5 \times 10^{-3}/f$
25 Hz−50 Hz	5	1.6×10^2	2×10^{-4}
50 Hz−400 Hz	$2.5 \times 10^2/f$	1.6×10^2	2×10^{-4}
400 Hz−3 kHz	$2.5 \times 10^2/f$	$6.4 \times 10^4/f$	$8 \times 10^{-2}/f$
3 kHz−10 MHz	8.3×10^{-2}	21	2.7×10^{-5}

Notes:
- f is the frequency in Hz.
- This table does not include non-sinusoidal and multiple frequency exposure.
- In the frequency range above 100 kHz, RF specific reference levels need to be considered separately.

Table B4. ICNIRP 2010 reference levels for occupational exposure to time varying electric and magnetic fields (unperturbed rms values) [17].

Frequency range	***E-field strength E (kV/m)***	***Magnetic field strength H (A/m)***	***Magnetic flux density B (T)***
1 Hz−8 Hz	20	$1.63 \times 10^5/f^2$	$0.2/f^2$
8 Hz−25 Hz	20	$2 \times 10^4/f$	$2.5 \times 10^{-2}/f$
25 Hz−300 Hz	$5 \times 10^2/f$	8×10^2	1×10^{-3}
300 Hz−3 kHz	$2.5 \times 10^2/f$	$2.4 \times 10^5/f$	$0.3/f$
3 kHz−10 MHz	1.7×10^{-1}	80	1×10^{-4}

Notes:
- f is the frequency in Hz.
- This table does not include non-sinusoidal and multiple frequency exposure.
- In the frequency range above 100 kHz, RF specific reference levels need to be considered additionally.

Appendix C – Protection of humans against electromagnetic effects. Comparing procedures suggested by IEC 61980 and ISO/PAS 19363 [2] [16].

Three protection areas around the vehicle are defined in order to define specific requirements for the exposure assessment (Figure C1):

- region 1: area underneath the vehicle (as large as the lower body width);
- region 2: area around the periphery of the vehicle;
- region 3: vehicle interior.

IEC 61980 adds the 'area of operation' as the space formed by the outline of the primary and secondary device using a different numbering.

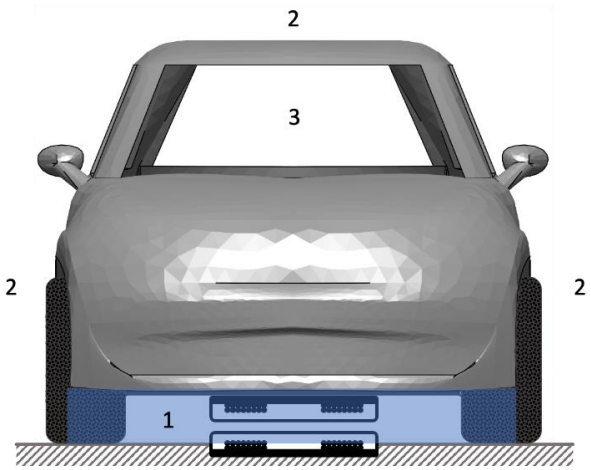

Figure C1. Protection areas.

In protection areas 2 and 3, the exposure at the worst-case alignment must be compliant with the limits at the frequencies of interest for WPT and are reported in Table C1 and Table C2.

Table C1. ICNIRP 2010 basic restrictions [17].

Quantity	ICNIRP 2010	
	RMS	**Peak**
Internal electric field	$1.35 \times 10^{-4} \times f(Hz) = 11$ V/m @81.38 kHz	$1.91 \times 10^{-4} \times f(Hz) = 15.5$ V/m @81.38 kHz

Table C2. ICNIRP 2010 reference levels [17].

Quantity	Unit	ICNIRP 1998	ICNIRP 2010
Magnetic field	µT	6.25	27
	A/m	5	21
Electric field	V/m	87	83

In protection areas 2 and 3, ISO/PAS 19363 further constrains the protection requirements in order to protect the functionality of active implantable medical devices (AIMDs). These limits are reported in Table C3. In the ISO/PAS 19363 document, region 2 is divided into two parts, below and above 70 cm, but the limits below 70 cm are less constraining than the corresponding ICNIRP level.

Table C3. Limits for AIMD protection (above 70 cm).

Protection Area	Magnetic field limits	
	RMS (information only)	**Peak (normative)**
2 and 3	15 µT or 11.9 A/m (81.38 kHz – 90 kHz)	21.2 µT or 16.9 A/m (81.38 kHz – 90 kHz)

B.1 Test procedures for exposure assessment

To assess the exposure to electromagnetic fields by humans, the standards define specific procedures.

The system must be regulated to obtain the maximum output power in normal non-faulty conditions, IEC 61980 allows the use of a correction factor in case this is not feasible. The gap between Tx and Rx and their alignment must be set to obtain the worst-case scenario. The ground assembly must be located on concrete or asphalt paved surface. Measurements must be performed in regions 2 and 3 only, with an isotropic 3-axis probe with a maximum sensor area of 100 cm^2.

In region 2, outside the vehicle, the test procedure involves the following steps (Figure C2):

1. set up system offset and gap conditions;

2. a sweep of the magnetic field probe around the boundary of region 1 (1/2 of the height of the 'floor'). IEC 61980 and ISO/PAS 19363 prescribes a lateral distance of 20 cm;

3. scan vertically and outward from region 1 to determine the maximum field. ISO/PAS 19363 specifies that starting from the point at the maximum emission value an appropriate extrapolation technique must be used to obtain the corresponding value at the vehicle perimeter. IEC 61980 requires a measurement for a period of at least 10 s in this position;

4. repeat for each combination of offset and gap conditions;

5. refinement of the test procedure if initial results are greater than 50 % of the exposure limit.

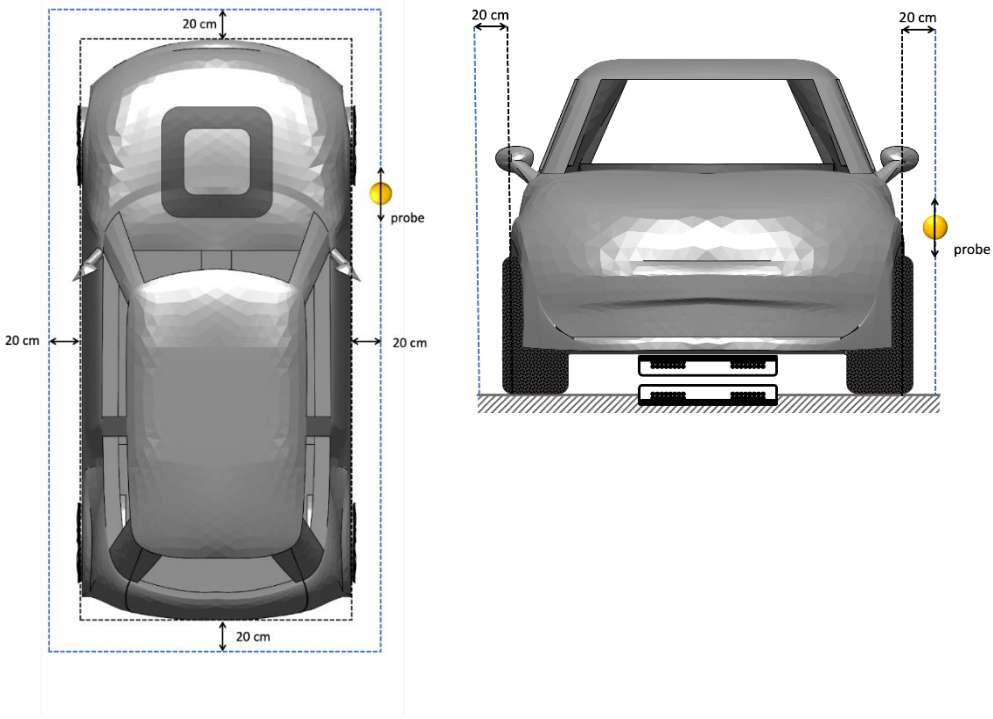

Figure C2. Region 2 geometry.

In region 3, inside the vehicle, the test procedure requires measurements to be made in the following positions (Figure C3):

a) head;
b) chest;
c) seat cushion;
d) foot.

The measurement must be repeated in order to identify the worst-case condition for the gap and offset.

Furthermore, IEC 61980 requires additional measurements for buses and minibuses at the location of the driver's seat and that of the seat closer to the secondary coil.

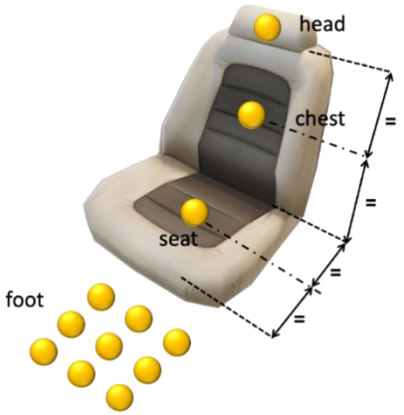

Figure C3. Region 3 test procedure.

Appendix D – Test case: a model with cylindrical symmetry

This Appendix reports a test case that can be useful for tuning an FEM model simulating the EMF generated by a WPT charging an electric vehicle. The test case was analysed by several partners of the MICEV project (and several computational codes), and the results are reported below.

It is a WPT system with cylindrical symmetry that includes an aluminium screen, a ferrite concentrator, a transmitting coil (Tx coil) and a receiving coil (Rx coil). Figures D1 and D2 illustrate the geometry. The dimensions in Figure 2 are in mm.

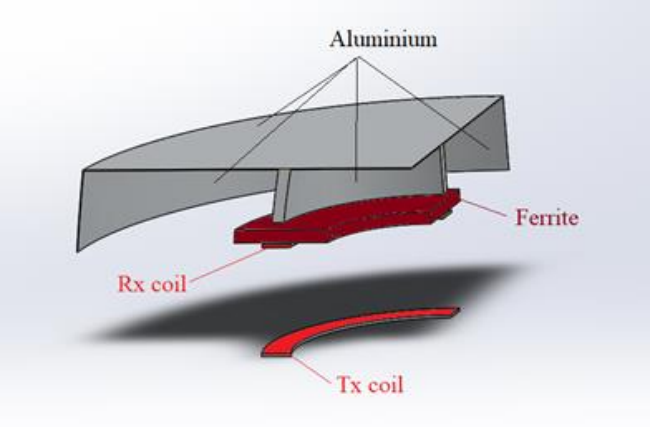

Figure D1. Double section (90 °) of the complete geometry (360°).

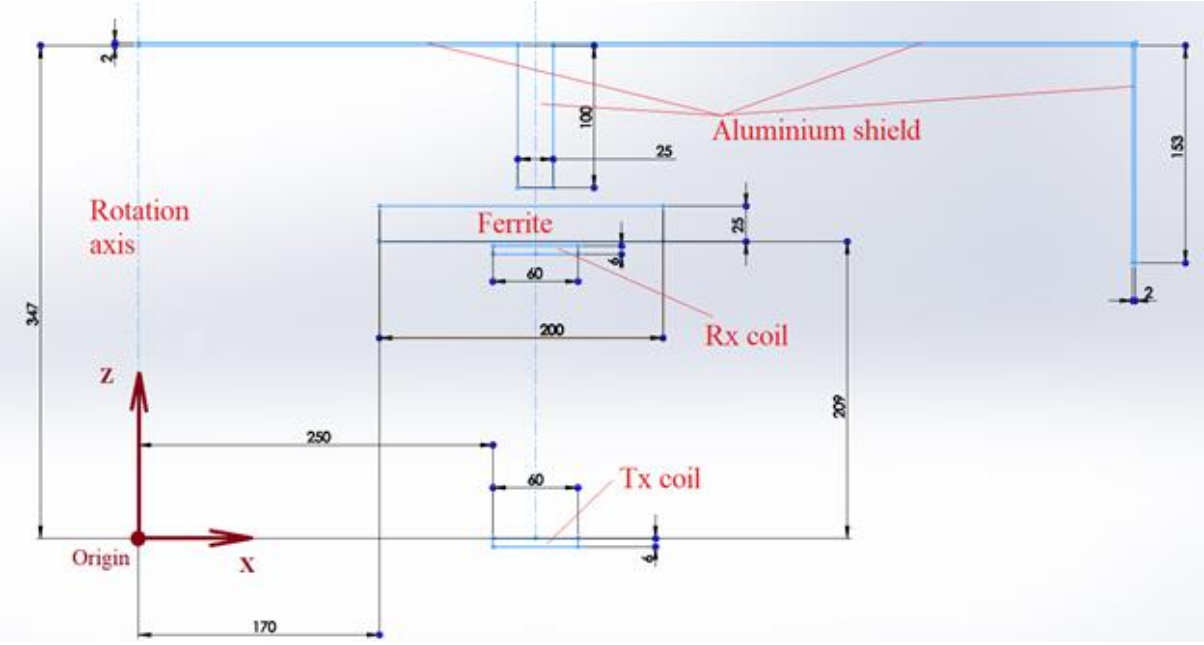

Figure D2. Basic geometry and dimensions in mm. The rotation axis is the Z-axis.

The material properties are summarised in Table D1. Table D2 summarises the power conditions, including current levels. Figure D3 summarises the results along the investigation line defined by: P1 (x = 1150; y = 0; z = 1150 mm) and P2 (x = 1150; y = 0; z = 2000 mm).

Table D1. Material properties.

Material	Conductivity (MS/m)	Relative permeability
Aluminium	33.45	1
Ferrite	0	2000

Table D2. Coil properties.

Coil	r.m.s. current (A)	Phase angle (degree)	no. of turns
Tx coil	50	0	10
Rx coil	105	-90	10

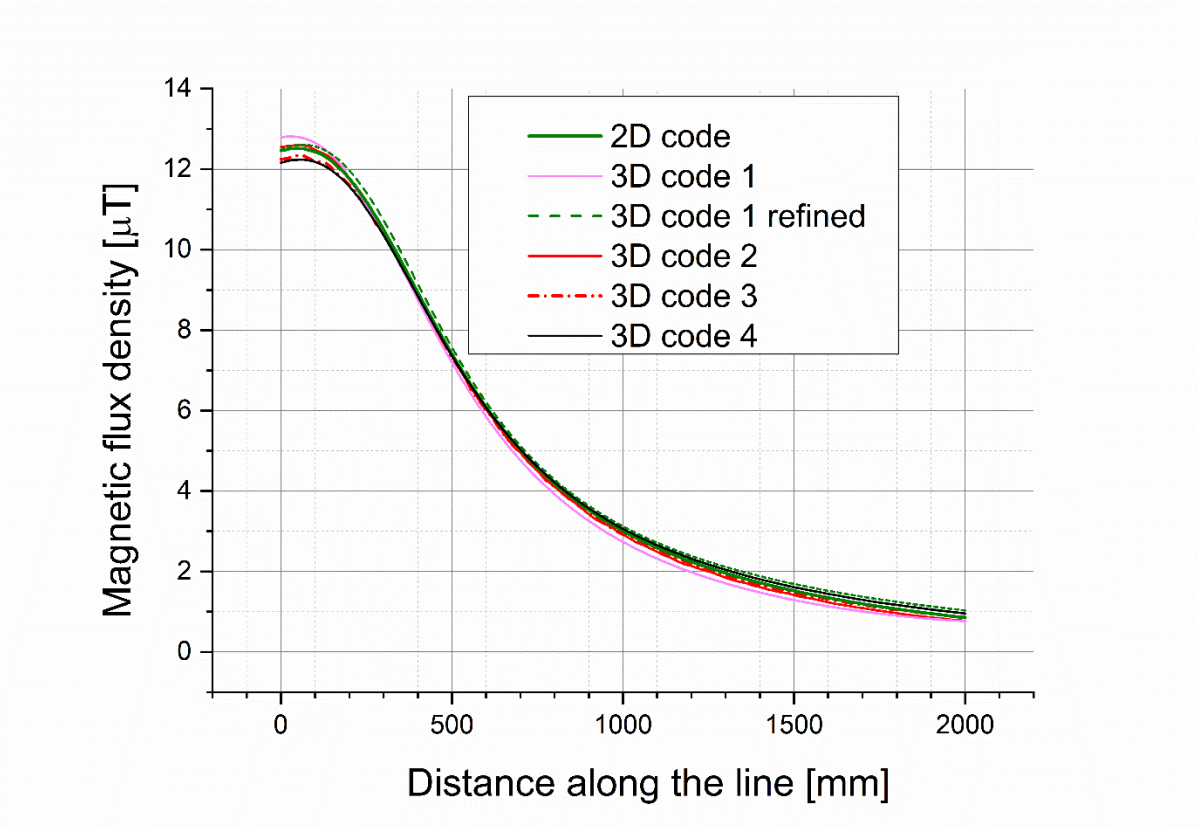

Figure D3. Computational results (flux density r.m.s. values) from different partners of the MICEV project. Peak values differ up to 8 %, depending on the mesh 3D and computational approach and convergence constraints.

All the datasets of the curves can be found at:
DOI: 10.5281/zenodo.4476252

Appendix E – Sensitivity of simulated exposure metrics to the variations in tissue properties

The demand for high-power wireless power transfer (WPT) systems for charging light and heavy electric vehicles is rapidly growing due to the industry adopting government strategies and future ambitions for electrification and de-carbonisation on the one hand, and the existing limitations of EV for long distance travel on the other. However, WPT systems can pose a safety risk when installed in uncontrolled environments. Within the framework of the European Project EMPIR-16ENG08 MICEV, a comprehensive experimental and numerical study was conducted to assess the general public exposure to WPT generated electromagnetic fields. To this end, the impact of uncertainty in tissue conductivities on the dosimetric result need to be quantified. According to [38], the measured data for the dielectric tissue models can vary by up to 25 % for frequencies below 100 kHz. The sensitivities here considered are valid for the low-frequency range below 1 MHz. Therefore, in addition to the other parameters listed in Table E1, the change in spatial-average specific absorption rate (psSAR) is also reported, for sake of completeness, although it has no direct interest for this guide.
In order to determine the associated uncertainty coefficients, a sensitivity analysis of the effect of the tissue conductivity on the overall uncertainty for the induced fields was performed. It is assumed that no high-conductivity (i.e. metallic) objects exist in the body, such as implanted medical devices and conductive prosthesis.
The goal of the analysis presented here was to provide estimates for the field and current variations in case tissue conductivity varies. Let us consider a WPT system that has a large primary coil with current I that produces an axisymmetric magnetic field $\mathrm{Bz}(\rho)$ around the centre of the coil (Figure E1a). The coil is embedded inside an infinite host medium with constant conductivity. In this example, it is shown that throughout such a homogeneous medium, under magneto-quasi-static (MQS) approximation, the electric field (E-field) is insensitive to conductivity changes.

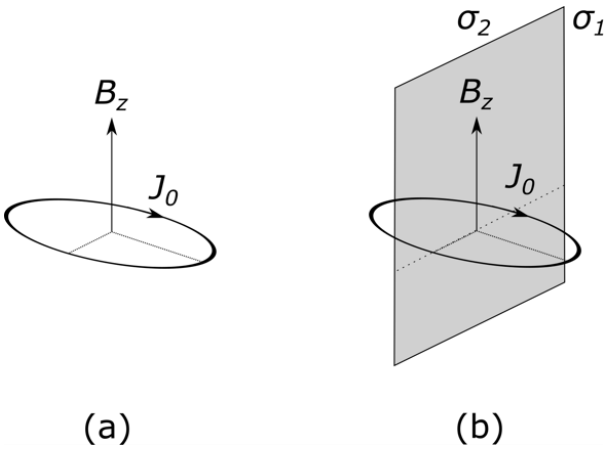

Figure E1. (a) Model for a current radiating magnetic field into a homogeneous medium, and (b) an extreme case where a conductivity contrast resides at the position of the maximum magnetic field value.

The MQS equation for the scalar potential, is:

$$\nabla \cdot (\sigma \nabla \varphi) = -j\,\omega\,\nabla \cdot (\sigma A_0)$$

where $A_0 = \frac{\mu_0}{4\pi}\int \frac{J_0(r)}{|r - r'|d^3 r'}$, with $J_0(r)$ being the excitation current density flowing at point r.

For a homogeneous medium considering that $\nabla \cdot E = j\omega \nabla \cdot A_0$, the electric field becomes independent from the surrounding material conductivity.

Therefore, the current density J is always proportional to the conductivity ($J \propto \sigma$) due to Ohm's law ($J = \sigma E$), meaning that:

$$\frac{\delta J}{J} = \frac{\delta \sigma}{\sigma}.$$

Furthermore, $\sigma E = J$ dictates that the electric field stays constant independent of the conductivity. The conclusion drawn is that the main source of electric field sensitivity to conductivity is the inhomogeneity of the material.

In the second step, an extreme case was considered where a conductivity change occurs over the maximum magnetic field of the large coil (Figure E1b). The symmetry of the problem along radial direction yields $E_\rho = E_z \approx 0$. Using the Maxwell-Faraday equation, the values for E_φ^1 (E-field in medium 1) and E_φ^1 (E-field in medium 2) are obtained as follows:

$$E_\varphi^1 = \frac{\sigma_2}{\sigma_1 + \sigma_2}\left(\frac{-2j\omega}{\rho}\int B_z(\rho)\rho d\rho\right) = \frac{\sigma_2}{\sigma_1 + \sigma_2}\, C(\rho)$$

$$E_\varphi^2 = \frac{\sigma_1}{\sigma_1+\sigma_2}\left(\frac{-2j\omega}{\rho}\int B_z(\rho)\rho d\rho\right) = \frac{\sigma_1}{\sigma_1+\sigma_2}\, C(\rho).$$

The current densities J_φ^1 and J_φ^2 are then obtained as:

$$J_\varphi^1 = J_\varphi^2 = \frac{\sigma_1\sigma_2}{\sigma_1+\sigma_2} C(\rho).$$

Here, we define the parameter $\left.\frac{\delta E_\varphi^i}{E_\varphi^i}\right|_j$ as the relative change in the electric field of medium *i* when the conductivity of the medium *j* changes. Using the above equations and the error estimate from $\delta f = \left(\frac{\partial f}{\partial \sigma}\right)\delta\sigma$, one obtains:

$$\left.\frac{\delta E_\varphi^1}{E_\varphi^1}\right|_1 = \frac{-\sigma_1}{\sigma_1+\sigma_2}\frac{\delta\sigma_1}{\sigma_1}, \quad \left.\frac{\delta E_\varphi^1}{E_\varphi^1}\right|_2 = \frac{\sigma_1}{\sigma_1+\sigma_2}\frac{\delta\sigma_2}{\sigma_2}$$

$$\left.\frac{\delta J_\varphi^1}{J_\varphi^1}\right|_1 = \frac{\sigma_2}{\sigma_1+\sigma_2}\frac{\delta\sigma_1}{\sigma_1}, \quad \left.\frac{\delta J_\varphi^1}{J_\varphi^1}\right|_2 = \frac{\sigma_1}{\sigma_1+\sigma_2}\frac{\delta\sigma_2}{\sigma_2}.$$

The above equations imply that the relative change in electric field and current density maximises to $\delta\sigma/\sigma$ when a large conductivity change exists, i.e. $\sigma_1 \gg \sigma_2$. Therefore, it can be deduced that:

$$\left.\frac{\delta J}{J}\right|_{max} = \left.\frac{\delta E}{E}\right|_{max} = \frac{\delta\sigma}{\sigma}.$$

Using the equation for $\left.\frac{\delta E_\varphi^1}{E_\varphi^1}\right|_1$, we can also obtain the maximum sensitivity of the specific absorption rate (SAR) to conductivity. From SAR definition, $SAR = \frac{\sigma E^2}{\rho}$, we obtain:

$$\frac{\delta SAR}{SAR} = \frac{\delta\sigma}{\sigma}\left(1 + 2\sigma\frac{E'(\sigma)}{E}\right)\frac{\delta\sigma}{\sigma}\left(1 + 2\frac{\delta E/E}{\delta\sigma/\sigma}\right).$$

Therefore, the maximum relative change in SAR is obtained as:

$$\left.\frac{\delta SAR}{SAR}\right|_{\max} = 3\frac{\delta\sigma}{\sigma}.$$

Using the above equations for the sensitivity of the electric field, current density and SAR, the maximum change due to an exemplary conductivity change of 20 % is shown to be 1.6 dB for the electric field and current density, and 2 dB for the SAR. In addition, an attempt has been made to validate this theory based on simulations over the entire human body.

The preliminary validation model for the theoretical approximation is depicted in Figure E2. It consists of an anatomical Virtual Population phantom, ViP, (IT'IS Foundation; see below), placed in front of a large wireless power transfer (WPT) coil [47] [48] [49] [50]. The coil consists of two concentric square loops with side lengths of 0.68 m and 0.7 m, which are excited by a 1 A current at 85 kHz. Although the validation model is simulated at 85 kHz, the evaluated sensitivities are valid for the whole low-frequency range below 1 MHz. This assumption holds since the IT'IS low-frequency (LF) database assumes a constant conductivity for tissues up to 1 MHz. Consequently, the induced current and the E-field produced varies proportionally with frequency thus the relative sensitivity does not change with frequency. It is intended that additional systematic configurations with variations of the induced current vector with respect to the tissue structure will be added in the future, to perform the full validation.

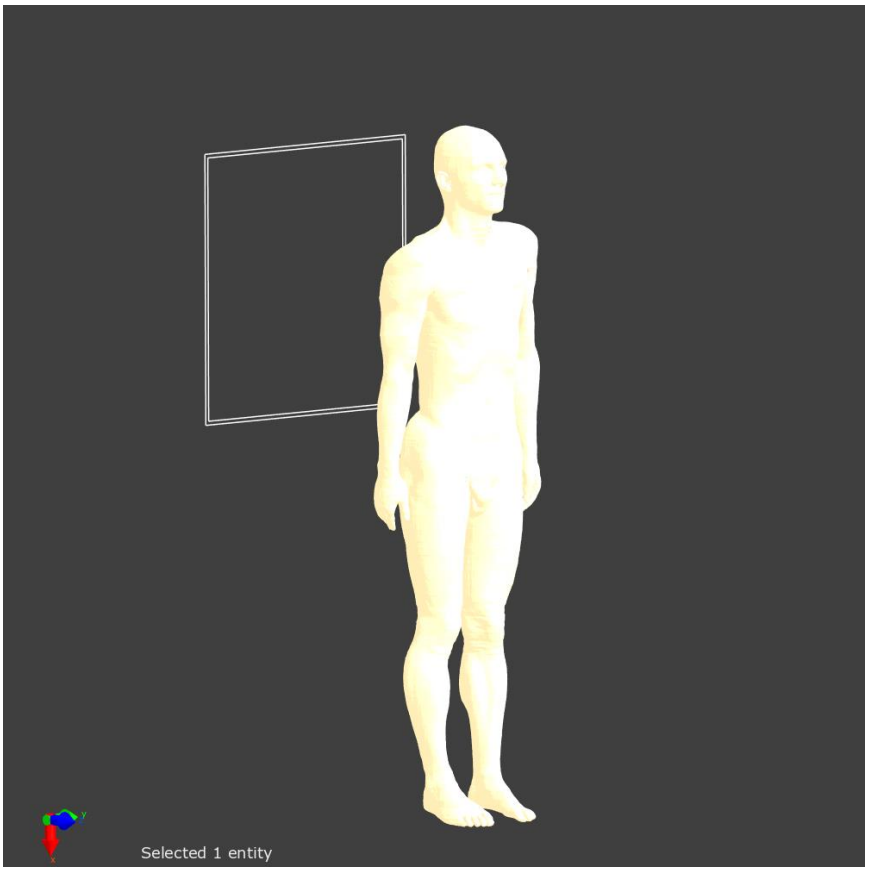

Figure E2. Simulation model including the Duke ViP Phantom in front of a WPT coil.

The validation model was created and simulated using the Sim4Life V5.0 simulation platform (Zurich Med Tech (ZMT) AG, Switzerland) to assess the exposure of the Duke ViP phantoms. Since the wavelength is much larger than the exposed object at the simulation frequency, i.e. 85 kHz, a quasi-static approximation was used. The Magneto-quasi-static electromagnetic solver of Sim4Life was used for the simulations.

The simulation grid only needs to discretise the anatomical phantoms, since the source is modelled through its analytical fields. Because of the large coil dimensions, the whole body is considered in a uniform cartesian grid with 1 mm resolution.

The advanced high-resolution anatomical ViP model Duke (BMI = 22.4 kg/m^2) was used to perform the numerical simulations. Tissue dielectric properties for the baseline were assigned according to the IT'IS Foundation LF Database. The conductivity of the skin tissue was 0.17 S/m to account for the dermis. Subsequently, throughout the sensitivity study the conductivity of five main tissues in the body, namely skin, fat, muscle, bone-cancellous, and bone-cortical, were changed in relative ratios of 2 %, 5 %, 10 % and 20 %.

The fields in the simulation model are excited through the vector potential analytically derived for the current coil.
In detail, the inhomogeneous Poisson equation $\nabla \cdot (\sigma \nabla \varphi) - j\,\omega\,\nabla \cdot (\sigma A_0)$ is solved, where σ is the material conductivity and A_0 is calculated by means of the of Biot-Savart law:

$$A_0(r) = \frac{\mu_0}{4\pi} \int \frac{J_0(r)}{|r-r'|} d^3r'.$$

To study the sensitivity of the exposure values based on different guidelines [3-5], the following parameters were extracted from the simulated fields:

- **peak cube-average electric field:** The induced electric field at any location r_0 is determined as a vector average of the electric field within a small contiguous tissue cubic volume of 2×2×2 mm^3 as $\langle E(r_0)\rangle_V\, 1/r \int E(r)\, dv$ where V is the volume of lossy tissue within the cube. The peak cube-average electric field is then the peak of the quantity $\langle E(r_0)\rangle_V$ over the computational phantom;
- **peak line-average electric field:** The induced electric field is averaged over a line of length 5 mm as $\langle E(r_0)\rangle_L = 1/L \int E(r) \cdot l_0\, dl$. The peak of this value over the whole computational phantom is considered as peak line-average electric field;
- **peak area-average current density:** Current density $J\ [A/m^2]$ is averaged by computing the current flow through a circular surface, S, perpendicular to the current direction n_0 at the centre point r_0 and dividing by its area. The averaged current density at each location is formulated as $\langle J(r_0)\rangle_S = \frac{1}{S} \int J(r) \cdot n_0\, ds$, where S is a circle with area 1 cm^2. The peak of this value over the computational phantom is defined as peak area-average current density;
- **psSAR1g:** is the peak spatial-average SAR over 1 g of the tissue considered;
- **psSAR10g:** is the peak spatial-average SAR over 10 g of the considered tissue considered.

The conductivities derived from IT'IS Foundation LF database, are tabulated in Table E1. The variations in the tabulated parameters due to changes in the conductivity of skin, fat, muscle, bone-cancellous, and bone-cortical are presented in Tables E2–E6, respectively.

Table E1. Values of the extracted parameters when no conductivity tissue is changed.

Peak cube-avg E [V/m]	0.1
Peak line-avg E [V/m]	0.077
Peak area-avg J [A/m2]	0.011
psSAR1g [W/kg]	3.1E-07
psSAR10g [W/kg]	2.5E-07

Table E2. Variations of the studied parameters due to the change in conductivity of the skin.

Conductivity variance (%)	-20	-10	-5	-2	+2	+5	+10	+20
ΔPeak cube-avg E [dB]	0.006	0.003	0.001	0.001	-0.001	-0.001	-0.002	-0.005
ΔPeak line-avg E [dB]	0.485	0.234	0.115	0.046	-0.045	-0.111	-0.219	-0.381
ΔPeak area-avg J [dB]	0.025	0.012	0.006	0.002	-0.002	-0.006	-0.012	-0.023
ΔpsSAR1g [dB]	0.029	0.014	0.007	0.003	-0.003	-0.007	-0.014	-0.028
ΔpsSAR10g [dB]	0.014	0.007	0.003	0.001	-0.001	-0.003	-0.007	-0.013

Table E3. Variations of the studied parameters due to the change in conductivity of the fat.

Conductivity variance (%)	-20	-10	-5	-2	2	5	10	20
ΔPeak cube-avg E [dB]	0.143	0.069	0.034	0.013	-0.013	-0.033	-0.064	-0.125
ΔPeak line-avg E [dB]	0.084	-0.034	-0.015	-0.006	0.005	0.012	0.021	0.031
ΔPeak area-avg J [dB]	0.085	0.041	0.020	0.008	-0.008	-0.020	-0.039	-0.069
ΔpsSAR1g [dB]	0.057	0.028	0.014	0.005	-0.005	-0.013	-0.027	-0.052
ΔpsSAR10g [dB]	-0.038	-0.018	-0.009	-0.004	0.004	0.009	0.018	0.035

Table E4. Variations of the studied parameters due to the change in conductivity of the muscle.

Conductivity variance (%)	-20	-10	-5	-2	2	5	10	20
ΔPeak cube-avg E [dB]	-0.90	-0.42	-0.20	-0.08	0.08	0.19	0.37	0.70
ΔPeak line-avg E [dB]	-0.37	-0.17	-0.08	-0.03	0.03	0.07	0.14	0.43
ΔPeak area-avg J [dB]	-0.97	-0.52	-0.29	-0.17	0.18	0.44	0.85	1.63
ΔpsSAR1g [dB]	-0.92	-0.47	-0.23	-0.09	0.09	0.22	0.43	0.85
ΔpsSAR10g [dB]	-0.90	-0.42	-0.21	-0.08	0.08	0.20	0.38	0.75

Table E5. Variations of the studied parameters due to the change in conductivity of the bone-cancellous.

Conductivity variance (%)	-20	-10	-5	-2	2	5	10	20
ΔPeak cube-avg E [dB]	0.34	0.17	0.08	0.03	-0.03	-0.08	-0.16	-0.32
ΔPeak line-avg E [dB]	0.043	-0.008	-0.004	-0.002	0.002	0.004	0.007	0.014
ΔPeak area-avg J [dB]	-0.012	-0.006	-0.003	-0.001	0.001	0.003	0.005	0.010
ΔpsSAR1g [dB]	0.003	-0.006	-0.003	-0.001	0.001	0.003	0.006	0.011
ΔpsSAR10g [dB]	-0.010	-0.005	-0.002	-0.001	0.001	0.002	0.005	0.009

Table E6. Variations of the studied parameters due to the change in conductivity of the bone-cortical.

Conductivity variance (%)	-20	-10	-5	-2	2	5	10	20
ΔPeak cube-avg E [dB]	0.39	0.19	0.09	0.04	-0.04	-0.09	-0.18	-0.36
ΔPeak line-avg E [dB]	0.00	0.00	0.00	0.00	0.00	0.00	0.00	0.00
ΔPeak area-avg J [dB]	0.00	0.00	0.00	0.00	0.00	0.00	0.00	0.00
ΔpsSAR1g [dB]	0.00	0.00	0.00	0.00	0.00	0.00	0.00	0.00
ΔpsSAR10g [dB]	0.00	0.00	0.00	0.00	0.00	0.00	0.00	0.00

The simulation results show that the studied exposure parameters are mostly sensitive to the conductivity of muscle, except for the peak line-average electric field which shows a slightly higher sensitivity to skin conductivity. This is in agreement with the proposed hypothesis that a large conductivity change leads to a high sensitivity to tissue properties. Skin and muscle are tissues with large conductivities and reside adjacent to tissues like bone-cortical and fat with low permittivity. It is recommended that all five tissue properties are studied for a complete sensitivity analysis. Nonetheless, only investigating the sensitivity to muscle conductivity yields reliable results for exposure safety analysis due to the maximum conductivity change between muscle and bone-cortical. In addition, the obtained relative changes are less than the theoretical maxima according to the hypothesis, which shows the validity of the developed hypothesis.

In this study, the effect of conductivity variations was investigated on the dosimetric levels observed in wireless power transfer systems. To account for a 25 % variation in tissue conductivity, the corresponding maximum change in the electric field and current density will be 1.9 dB. The change in SAR is 2.4 dB. In examples where these uncertainties are detrimental to a specific system design, a more accurate (less conservative) uncertainty value is needed. A comprehensive sensitivity analysis needs to be performed including all tissues in the exposed volume.

Appendix F – EURAMET NMI's with AC magnetic field capability at the frequency range of interest for WPTs

The information given below was accurate as of January 2021. All data listed in the KCDB has been reviewed and approved within the CIPM Mutual Recognition Arrangement and can be obtained from the CIPM MRA database hosted on the BIPM website: https://www.bipm.org.

Czech Republic, CMI (Czech Metrology Institute)

AC magnetic flux density: 1.00E-3 mT to 0.15 mT Relative expanded uncertainty: 2.0E-2 Frequency: 50 kHz to 100 kHz Approved on 07 February 2019 Institute service identifier: EMF14

AC magnetic flux density: 1.00E-3 mT to 1000 mT Relative expanded uncertainty: 6.0E-3 to 1.5E-2 Frequency: 10 Hz to 50 kHz Approved on 07 February 2019 Institute service identifier: EMF05a

Germany, PTB (Physikalisch-Technische Bundesanstalt)

AC magnetic flux density: 1 µT to 450 µT Relative expanded uncertainty: 2.0E-2 to 1.0E-3 Frequency: < 30 kHz Approved on 21 October 2001 Institute service identifier: 2.5.448

Italy, INRIM (Istituto Nazionale di Ricerca Metrologica)

AC magnetic flux density: 0.1 µT to 3000 µT Relative expanded uncertainty: 4 mT/T to 2.4E1 mT/T Frequency: 10 Hz to 100 kHz Approved on 07 April 2016 Institute service identifier: INRIM/208

Netherlands, VSL (VSL)

AC magnetic flux density: 1 µT to 2.00E4 µT Relative expanded uncertainty: 5 mT/T to 2.7E1 mT/T Frequency: 10 Hz to 100 kHz Approved on 07 April 2016 Institute service identifier: VSL/91

Poland, GUM (Glowny Urzad Miar, Central Office of Measures)

AC magnetic flux density: 5.00E-4 mT to 11 mT Relative expanded uncertainty: 0.5 % to 2.5 % Frequency: 10 Hz to 30 kHz Approved on 11 May 2017 Institute service identifier: GUM/29z

United Kingdom, NPL (National Physical Laboratory)

AC magnetic flux density: 1.00E-8 T to 0.022 T Relative expanded uncertainty: 0.25 % to 0.7 % Frequency: 10 Hz to 120 kHz Approved on 06 August 2013 Institute service identifier: 316

AC field calibration system within the framework of the MICEV project. The following outlines the new capability, but it is not yet listed on the CIPM MRA database:

Maximum field capability:	DC to 50 kHz: 100 µT 50 kHz < f ≤ 100 kHz: 50 µT 100 kHz < f ≤ 150 kHz: 23 µT 150 kHz < f ≤ 250 kHz: 7.25 µT
Expanded uncertainty (k=2):	± 0.5 % at 1 kHz ± 1.0 % at 150 kHz

End of document